AD-A244 001

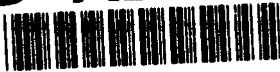

Annual Letter Report

DTIC
ELECTE
S C D

Pseudomorphic Semiconducting Heterostructures from Combinations of AlN, GaN and Selected SiC Polytypes: Theoretical Advancement and its Coordination with Experimental Studies of Nucleation, Growth, Characterization and Device Development

Supported under Grant #N00014-90-J-1427
Department of the Navy
Office of the Chief of Naval Research
Report for the period January 1, 1991–December 31, 1991

Robert F. Davis, Zlatko Sitar, Scott Kern, Larry Rowland,
Joe Sumakeris and Satoru Tanaka
Materials Science and Engineering Department
North Carolina State University
Campus Box 7907
Raleigh, NC 27695-7907

91-19111

December, 1991

DISTRIBUTION STATEMENT A
Approved for public release;
Distribution Unlimited

91 12 20 022

REPORT DOCUMENTATION PAGE	Form Approved OMB No 0704-0188

Public reporting burden for this collection of information is estimated to average 1 hour per response, including the time for reviewing instructions, searching existing data sources, gathering and maintaining the data needed, and completing and reviewing the collection of information. Send comments regarding this burden estimate or any other aspect of this collection of information, including suggestions for reducing this burden, to Washington Headquarters Services, Directorate for Information Operations and Reports, 1215 Jefferson Davis Highway, Suite 1204, Arlington, VA 22202-4302, and to the Office of Management and Budget, Paperwork Reduction Project (0704-0188), Washington, DC 20503.

1. AGENCY USE ONLY (Leave blank)

2. REPORT DATE
December, 1991

3. REPORT TYPE AND DATES COVERED
Annual Letter 1/1/91–12/31/91

4. TITLE AND SUBTITLE
Pseudomorphic Semiconducting Heterostructures from Combinations of AlN, GaN and Selected SiC Polytypes: Theoretical Advancement and its Coordination with Experimental Studies

5. FUNDING NUMBERS
414s007---01
1114SS
N00179
N66005
4B855

6. AUTHOR(S)
Robert F. Davis

7. PERFORMING ORGANIZATION NAME(S) AND ADDRESS(ES)
North Carolina State University
Hillsborough Street
Raleigh, NC 27695

8. PERFORMING ORGANIZATION REPORT NUMBER
N00014-90-J-1427

9. SPONSORING/MONITORING AGENCY NAME(S) AND ADDRESS(ES)
Department of the Navy
Office of the Chief of Naval Research
800 North Quincy, Code 1513:CMB
Arlington, VA 22217-5000

10. SPONSORING/MONITORING AGENCY REPORT NUMBER

11. SUPPLEMENTARY NOTES

12a. DISTRIBUTION/AVAILABILITY STATEMENT
Approved for Public Release; Distribution Unlimited

12b. DISTRIBUTION CODE

13. ABSTRACT (Maximum 200 words)

Cubic solid solutions of AlN and SiC have been epitaxially deposited for the first time in this film form on β-SiC films grown on Si(100) using gas-source molecular beam epitaxy (GSMBE). Specific studies of the deposition of unintentionally-doped beta-SiC on Si(100) and Al-doped beta-SiC on alpha (6H)-SiC(0001) have also been achieved via GSMBE. Cross-sectional TEM confirmed the epitaxial growth of the three types of films. A low concentration of double positioning boundaries was observed in the material deposited on α(6H)-SiC. The initial stages of nucleation and thin film growth of AlN and GaN on sapphire and α(6H)-SiC single crystals were also investigated. No significant changes in the substrate surface chemistry was observed for growth on sapphire; however, Si_4N_4 was observed on the SiC surface as a result of ion bombardment prior to deposition. The growth of GaN on sapphire followed a Stranski-Krastanov growth mode, while on SiC, it appeared to be three-dimensional. By contrast, AlN grew on both substrates initially by a layer-by-layer mode. Ultraviolet radiation during deposition did not produce any significant changes in the nucleation and growth of these materials.

14. SUBJECT TERMS
pseudomorphic heterostructures, cubic SiAlCN solid solutions, beta-SiC, alpha (6H)-Si, gallium nitride, aluminum nitride, gas-source molecular beam epitaxy

15. NUMBER OF PAGES
42

16. PRICE CODE

17. SECURITY CLASSIFICATION OF REPORT	18. SECURITY CLASSIFICATION OF THIS PAGE	19. SECURITY CLASSIFICATION OF ABSTRACT	20. LIMITATION OF ABSTRACT
UNCLAS	UNCLAS	UNCLAS	SAR

Table of Contents

I. Introduction 1

II. Growth of AlN-SiC Solid Solutions on Si Using a β-SiC Intermediate Layer by Gas-Source Molecular Beam Epitaxy 2
- A. Introduction 2
- B. Experimental Details 2
- C. Results and Discussion 3
- D. Conclusions 7
- E. Future Work 8
- F. References 8

III. Growth and Characterization of β-SiC Films Grown on Si by Gas-Source Molecular Beam Epitaxy 9
- Abstract 9
- 1. Introduction 9
- 2. Experimental Procedures 10
- 3. Results and Discussion 11
- 4. Conclusions 14
- Acknowledgements 15
- References 15

IV. Gas-Source Molecular Beam Epitaxy of Al-Doped β-SiC on 6H-SiC 16
- A. Introduction 16
- B. Experimental Details 17
- C. Results 18
- D. Discussion 21
- E. Conclusions 22
- F. Future Work 22
- G. References 22

V. Interface Chemistry and Surface Morphology in the Initial Stages of Growth of GaN and AlN on a-SiC and Sapphire 24
- A. Introduction 24
- B. Experimental Procedures 26
  - 1. Deposition System 26
  - 2. Film Growth 27
  - 3. XPS Analysis 28
- C. Results and Discussion 31
  - 1. Growth Morphology: GaN 31
  - 2. Growth Morphology: AlN 34
  - 3. Interface Chemistry: GaN 35
  - 4. Interface Chemistry: AlN 37
- D. Conclusions 41
- E. Future Research Plans 42
- F. References 42

Accession For
NTIS GRA&I
DTIC TAB
Unannounced
Justification
By
Distribution/
Availability Codes
Avail and/or
Dist Special
A-1

I. Introduction

The advent of techniques for growing semiconductor multilayer structures with layer thicknesses approaching atomic dimensions has provided new systems for both basic physics studies and device applications. Most of the research involving these structures has been restricted to materials with lattice constants that are equal within $\simeq 0.1\%$ However it is now recognized that interesting and useful pseudomorphic structures can also be grown from a much larger set of materials that have lattice-constant mismatches in the percent range. Moreover, advances in computer hardware and software as well as the development of theoretical structural and molecular models applicable for strained layer nucleation, growth and property prediction have occurred to the extent that the field is poised to expand rapidly. It is within this context that the research described in this report is being conducted. The materials systems of concern include combinations of the direct bandgap materials of AlN and GaN and selected, indirect bandgap SiC polytypes.

The extremes in thermal, mechanical, chemical and electronic properties of SiC allow the types and numbers of current and conceivable applications of this material to be substantial. However, a principal driving force for the current resurgence of interest in this material, as well as AlN and GaN, is their potential as hosts for high power, high temperature microelectronic and optoelectronic devices for use in extreme environments. The availability of thin film heterostructural combinations of these materials will substantially broaden the applications potential for these materials. The pseudomorphic structures produced from these materials will be unique because of their chemistry, their wide bandgaps, the availability of indirect/direct bandgap combinations, their occurrence in cubic and hexagonal forms and the ability to tailor the lattice parameters and therefore the amount of strain and the physical properties via solid solutions composed of the three components.

The research described in the following subsections constitutes the initial phases of material growth in this program following a prolonged period of equipment fabrication, testing and reconfiguration. Specifically, (1) the first cubic AlN-SiC solid solutions have been deposited via gas-source MBE in thin film form on β-SiC intermediate films (also produced in this study) previously deposited on Si substrates. Heavily Al-doped β-SiC films have also been grown on α(6H)-SiC wafers. Finally, the initial stages of nucleation and growth of AlN and GaN on sapphire and α(6H)-SiC substrates have been discussed. The following subsections detail the experimental procedures for each of the aforementioned studies, discuss the results and provide conclusions and references for these studies.

II. Growth of AlN-SiC Solid Solutions on Si Using a β-SiC Intermediate Layer by Gas-Source Molecular Beam Epitaxy

A. Introduction

Interest in wide-bandgap semiconductors for electronic and optoelectronic applications has increased greatly within the past several years. Two wide-bandgap materials which have generated much interest are SiC and AlN. SiC, the only binary compound in the Si-C system, is a prime candidate for high-power, high-temperature, and high-frequency electronic applications. It can form in many different polytypes; the most common of these are the cubic polytype, β- or 3C-SiC, and one of the hexagonal polytypes, 6H-SiC. However, since the bandgap (2.86 eV for 6H-SiC, and 2.28 eV for β-SiC) is indirect, SiC cannot be used alone for optoelectronic applications. AlN is of particular interest for ultraviolet optical devices due to its large, direct bandgap (E_g=6.28 eV). Typically, it forms in the wurtzite structure, although recent research showing cubic GaN grown on β-SiC [1] or GaAs [2] suggests the feasibility of growing cubic AlN films. Indeed, cubic AlN has been grown at NCSU [3] on β-SiC with the former having a thickness of ≈140 Å (the critical thickness has been calculated to be 143 Å[4] .

Research in ceramic systems suggests that complete solid solubility of AlN in SiC may exist [5]. This indicates the feasibility of forming thin-film solid solutions of AlN and SiC for microelectronic and optoelectronic applications. Assuming that complete solid solubility exists, bandgap engineering from 2.8-6.2 eV would be possible. In addition, these two materials are fairly close in lattice parameter. In the cubic form, for example, a_{SiC}= 0.4395 nm and a_{AlN}=0.438 nm (estimated by scaling from c/a ratios of GaN) [4]. This results in a lattice mismatch of about 0.6%. In Ref. 5, the critical layer thickness prior to misfit dislocation formation was calculated for cubic AlN on SiC to be 14.1 nm. Due to the potential applications of solid solutions and pseudomorphic structures of these two materials, a MBE/ALE system was commissioned, designed, and constructed for growth of structures and solid solutions of these two materials. In this report, evidence is presented which confirms the formation of cubic solid solutions of AlN and SiC on off-axis Si (001). The initial attempts regarding the formation of monocrystalline AlN and SiC layers on Si and SiC substrates are also described.

B. Experimental Details

The films containing Al, Si, N and C were grown on low-resistivity (ρ=.002-.004 Ω-cm), As-doped Si substrates cut 3.5 ± 0.5° off (001) toward [011]. Films were deposited using the gas source MBE system detailed in previous reports, and readers are referred to these reports for a description and schematic of the system. The material sources used are as follows: Si_2H_6 for silicon, C_2H_4 for carbon, activated nitrogen species produced in an ASTeX Compact ECR electron cyclotron resonance (ECR) plasma source from molecular nitrogen, and metallic Al

evaporated using a standard MBE effusion. The Si(100) substrates were chemically cleaned prior to growth using the following chemistries and sequence: H_2SO_4 at 70°C for 5 min; DI water rinse for 1 min; 1:1 solution (by volume) of 50% H_2O_2 and NH_4OH at 70°C for 5 min; DI water rinse for 1 min; BOE etch at room temperature for 5 min; and DI water for 2 min.

A thin converted layer of β-SiC was initially formed on Si(100) substrate by exposure of the substrate to 0.5 sccm C_2H_4 at 925°C for 15 min. Formation of this layer is be necessary for growth of relatively thick (< 30 μm), crack-free β-SiC films on Si [6-8]. Subsequently, a layer of monocrystalline β-SiC was formed by GSMBE on the converted layer using these conditions: Si_2H_6 flow, 1.0 sccm; C_2H_4 flow, 2.0 sccm; temperature, 1025°C; and time, 95 min. The AlN-SiC solid solutions were grown on the SiC films using the gases and flow rates of Si_2H_6 at 0.1 sccm, C_2H_4 at 2.0 sccm; and N_2 at 8 sccm; an Al source temperature of 1204°C; a sample temperature of 1025°C and time of 270 min. The chamber pressure during the deposition of the SiC intermediate layer was 6×10^{-5} torr; that during growth of the solid solutions and the separate AlN layers was 3×10^{-4} torr.

The surface morphology of these resultant structures was examined using optical microscopy and field-emission scanning electron microscopy (SEM). Chemical depth profiles of selected samples were obtained by Auger electron spectroscopy. Electron energy windows were determined for each of the constituent elements and used to find relative intensities for each element. These intensities were then adjusted for relative Auger electron yields for each element, resulting in relative concentrations of the elements in question as a function of depth. This analysis was performed using a JEOL JAMP-30 scanning Auger microprobe. Films which showed a Si:C ratio and Al:N ratio approximately that of each compound, if analyzed, separately were examined using high-resolution transmission electron microscopy (HRTEM). An Akashi EM 002B HRTEM was used for this purpose.

C. Results and Discussion

An Auger depth profile of the AlN-SiC sample is shown in Figure 1. Note that the relative concentrations of each component stay essentially constant through the SiAlCN solid solution. In Figure 2, a pure polycrystalline AlN standard is shown for comparison. The presence of Si in the solid solution in the film is evident in Figure 1. The peak used to determine the relative concentration of C in this analysis is much less sensitive than the Si KLL peak used to monitor Si. This explains the apparent lack of C in this film. Additional analysis schemes are needed to determine the concentration of C in the AlN-SiC layer.

From the viewpoint of microstructure, the final surface of the solid solutions sample appeared smooth in optical microscopy except for the presence of 0.5-1.0 μm diameter pits on the growth surface which extend into the Si substrate. Examination of samples with SEM

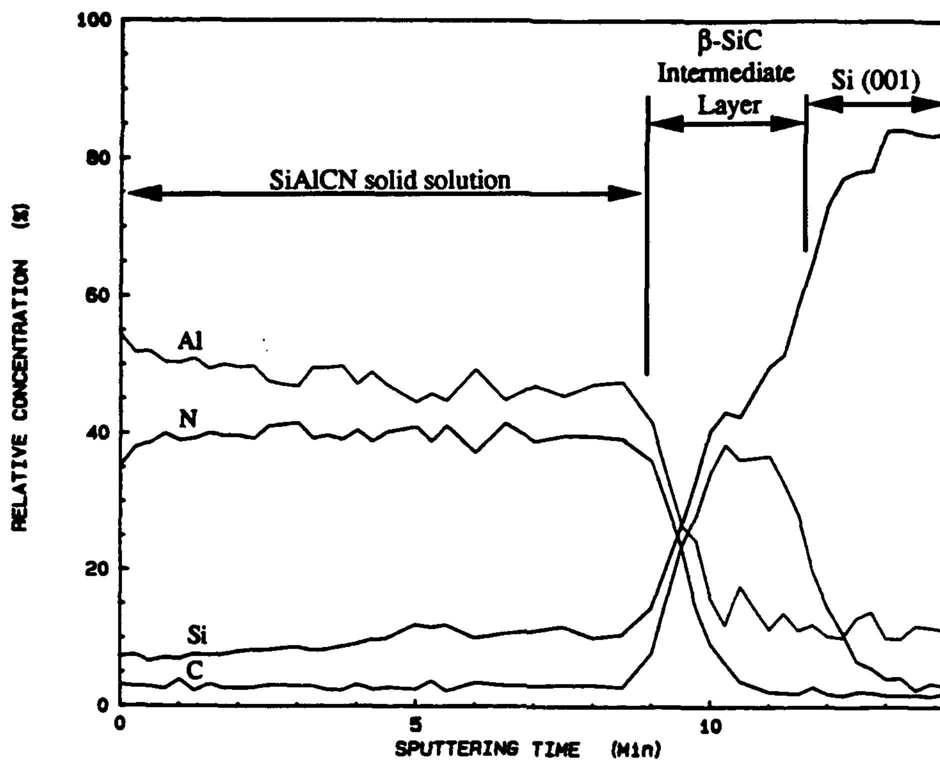

Figure 1. Auger depth profile of AlN-SiC and SiC films on Si substrate.

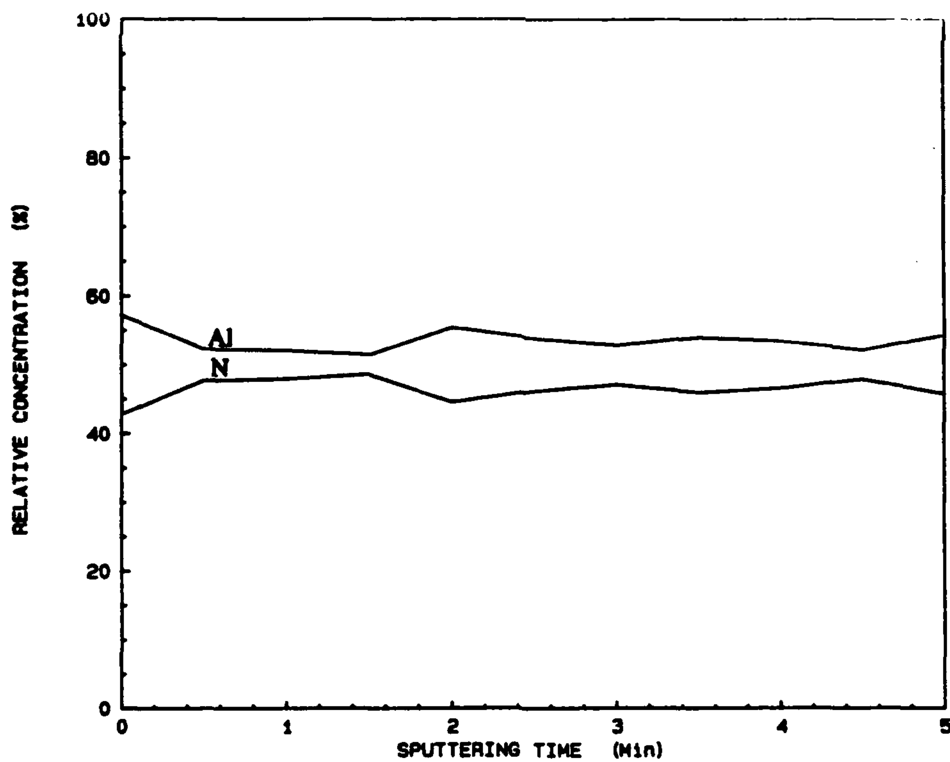

Figure 2. Auger depth profile of AlN standard.

showed, however, that the grown surface was fairly rough and platelike between these pits. An example of this is shown in Fig. 3. Examination of the surfaces of pure β-SiC films grown Si(100) using this system as well as via CVD show these same pitted features; thus, they do not result solely from the deposition of the SiAlCN solid solutions.

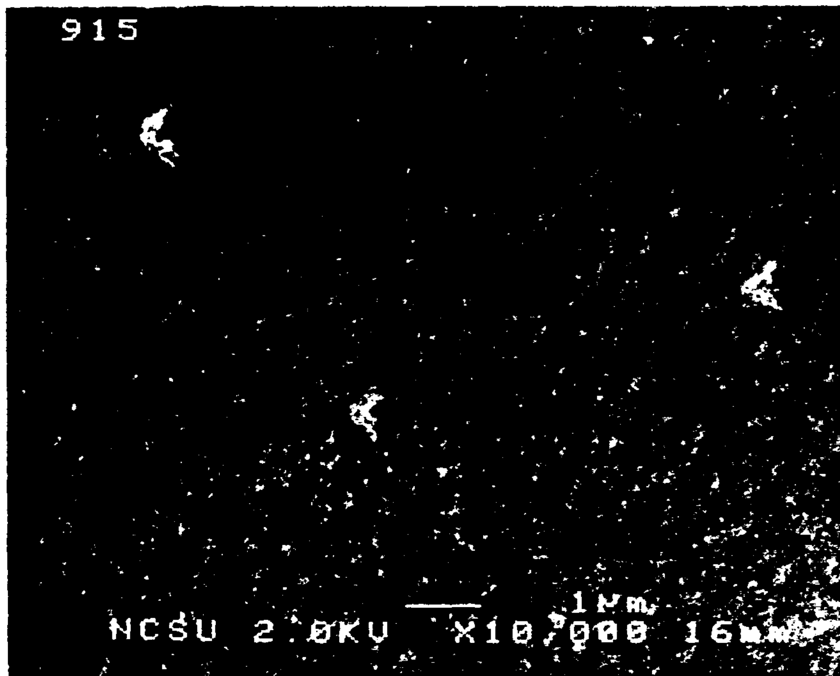

Figure 3: Surface morphology of AlN-SiC film by field-emission SEM.

Cross-section HRTEM was performed on this sample to structurally examine the layers. A HRTEM micrograph showing the SiAlCN layer, the β-SiC intermediate layer, and the Si substrate is presented in Figure 4. The β-SiC (100) layer is epitaxial with the Si(100) substrate, though many <111> microtwins can be seen as a result of the 20% lattice mismatch. The interface between the SiAlCN layer and the β-SiC film can be observed, though it is not atomically abrupt throughout the entire area shown in the micrograph. The SiAlCN layer is polycrystalline, though some regions appear to have an epitaxial relationship to the SiC layer. Near the surface, the sample appears to be amorphous. This may be due to damage induced during the ion milling process necessary for cross-sectional TEM sample preparation. An interesting aspect of this SiAlCN layer is that the vast majority of grains have lattice fringes corresponding to a cubic crystal structure.

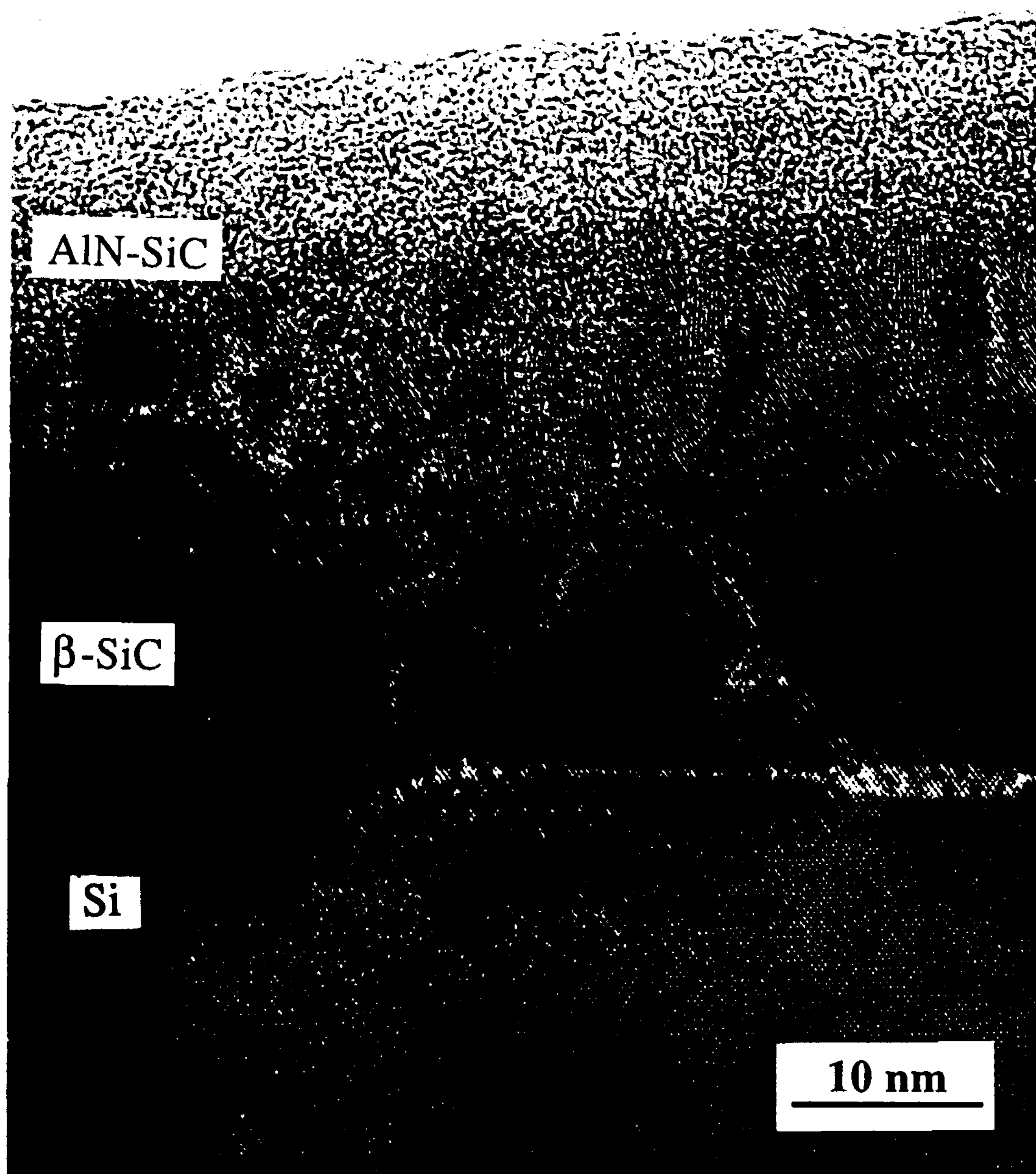

Figure 4: Cross-sectional HRTEM image of AlN-SiC and β-SiC films on Si substrate.

Figure 5 shows an electron diffraction pattern of the film and substrate taken during this analysis. If diffraction spots corresponding to Si and SiC (110) poles are eliminated, then a ring pattern remains. This ring pattern corresponds to the cubic SiAlCN polycrystalline layer. Although a small amount of cubic phase has been observed in previous SiAlCN solid solutions obtained by hot-pressing SiC and AlN [5], these layers grown by MBE appear to be completely cubic.

The microstructure of the solid solution consists of very small grains (on the order of 2-5 nm in width). If grains of this size existed in the film consisting of AlN and SiC with little solid solubility between the two, all other things being ideal, the mismatch between AlN and SiC is sufficiently small so that coherent interfaces between the grains would form. There must be some other factor other than miscibility considerations which causes this nanocrystalline behavior. The top interface of the β-SiC film on Si appears to be quite rough. This roughness could cause nuclei of the solid solution to form at different orientations. If these misoriented nuclei formed, then nanocrystalline grain growth would most likely result. Experiments are planned for solid solution formation on β-SiC films grown on 6H-SiC substrates by GSMBE.

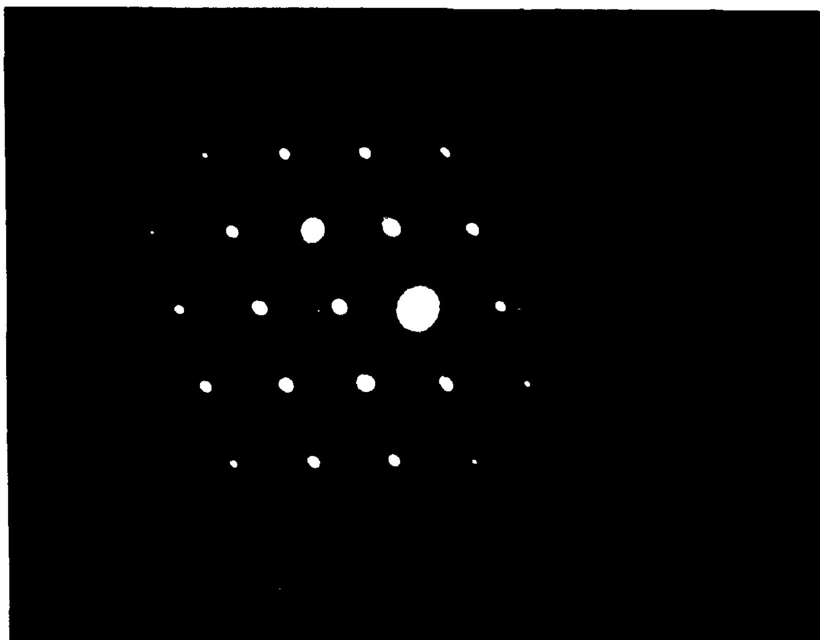

Figure 5: Selected area diffraction pattern of the SiAlCN solid solution and β-SiC films and the Si substrate.

D. Conclusions

Chemical and microstructural evidence is presented which confirms the formation of a polycrystalline cubic solid solution of AlN and SiC. It is speculated that surface roughness in the β-SiC intermediate "substrate" layer results in the polycrystallinity of the solid solution layer. Good-quality epitaxial β-SiC films on 6H-SiC (0001) substrates recently obtained using this MBE system will be used to provide a much smoother template on which to grow epitaxial solid solutions of various concentrations of AlN and SiC.

E. Future Work

Additional growth experiments are planned to determine the optimum growth parameters for the deposition of SiAlCN epitaxial solid solutions on both MBE-grown β-SiC (111) films on α(6H)-SiC(0001) substrates and directly on the 6H-SiC substrates. In addition, alternating layers of AlN and SiC will be grown on these substrates in order to obtain pseudomorphic structures of these two materials. These layers will be analyzed chemically, structurally, and electrically to determine properties of both the solid solutions and the pseudomorphic layers.

F. References

1. M. J. Paisley, Z. Sitar, J. B. Posthill, and R. F. Davis, J. Vac. Sci. Technol. **A 7**, 701 (1989).
2. M. Mizuta, S. Fujieda, Y. Matsunomo, and T. Kawamura, Jpn. J. Appl. Phys **25**, L945 (1986).
3. Z. Sitar, Ph.D. Dissertation, North Carolina State University, Raleigh, NC, 1990.
4. See, for example, R. Ruh and A. Zangvil, J. Am. Ceram. Soc. **65**, 260 (1982).
5. M. E. Sherwin and T. J. Drummond, J. Appl. Phys. **69**, 8423 (1991).
6. S. Nishino, J. A. Powell, and H. A. Will, Appl. Phys. Lett. **42**, 460 (1983).
7. K. Sasaki, E. Sakuma, S. Misawa, S. Yoshida, and S. Gonda, Appl. Phys. Lett. **45**, 72 (1984).
8. P. Liaw and R. F. Davis, J. Electrochem. Soc. **132**, 642 (1985).

III. Growth and Characterization of β-SiC Films Grown on Si by Gas-Source Molecular Beam Epitaxy*

L. B. Rowland, S. Tanaka, R. S. Kern, and R. F. Davis

North Carolina State University, Department of Materials Science and Engineering, Box 7907, Raleigh, NC 27695-7907

Abstract. Films of β-SiC have been grown on 4° off-axis Si (100) substrates from 1198 to 1398 K by gas-source MBE using Si_2H_6 and C_2H_4. Monocrystalline films were obtained at temperatures as low as 1248 K, as confirmed by electron diffraction. The latter films were specularly reflective. However, SEM revealed growth pits extending to the SiC surface as well as preferential growth on the pit edges. Cross-sectional TEM analysis confirmed the epitaxial relationship between the film and the Si substrate. Misfit dislocations and microtwins were also observed.

1. Introduction

At present, economics and availability make Si and a two-step chemical vapor deposition (CVD) the most commonly used substrate and process route for the growth of SiC films. However, mismatches in lattice parameters and coefficients of thermal expansion of 20% and 8%, respectively, exist between the two materials. The CVD process involves the reaction of the Si substrate surface with a C-containing gaseous species to form a "converted" layer of β-SiC [1] prior to subsequent deposition of the β-SiC film using both C- and Si-containing precursors.

However, the high growth temperatures and level of control of growth parameters and doping species obtained with CVD have sparked interest in the technique of gas-source molecular beam epitaxy (GSMBE) for growth of SiC [2-4]. The latter technique allows for precise control of growth parameters and minimization of sample contamination during deposition and was used in the studies described below. Experiments were conducted to determine the feasibility of SiC growth directly on Si (100) and to offer a comparison to films to be grown on converted layers in the near future. Effects of the C_2H_4/Si_2H_6 ratio and growth temperature on film morphology and quality were examined.

* Preprint of paper accepted for publication in the *Proceedings of the Third International Conference on Amorphous and Crystalline Silicon Carbide.*

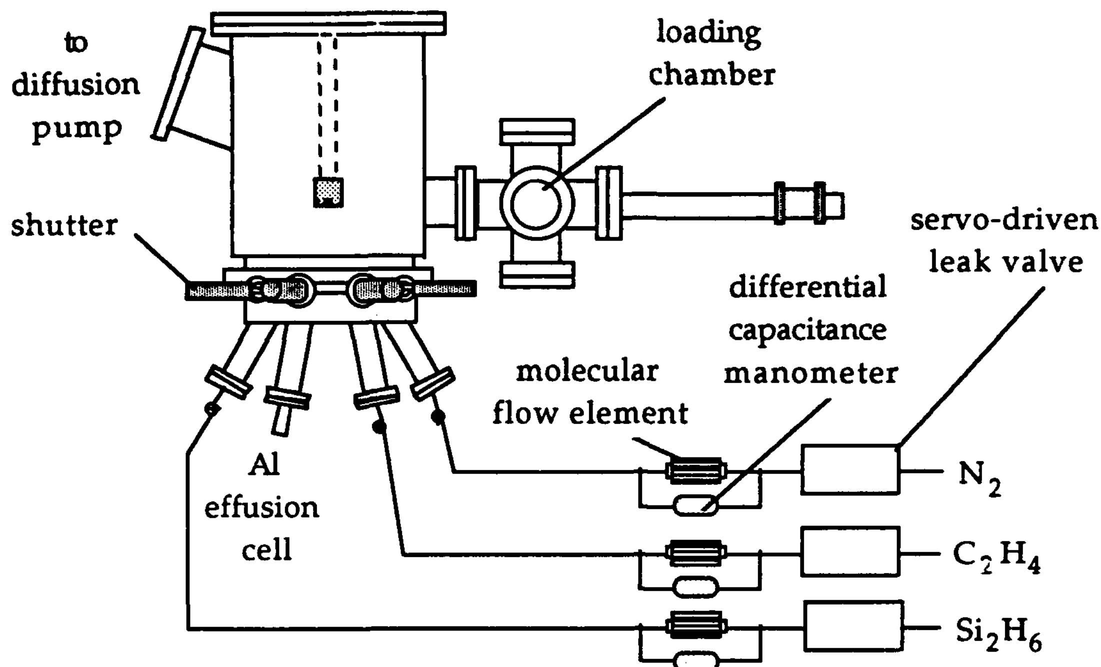

Figure 1. Schematic of molecular beam epitaxy apparatus

2. Experimental Procedures

Growth experiments were conducted using Si substrates primarily cut 4° off (100) toward the [011] direction. The use of off-axis substrates eliminates inversion domain boundaries (IDB's) [5,6]. The chemically cleaned (5 min H_2SO_4 (60°C), 1 min DI rinse, 5 min 1:1 H_2O_2/NH_4OH (60°C), 1 min DI rinse, 5 min BOE, 1 min DIrinse) substrates were introduced into the growth chamber shown in Figure 1 (6 x 10^{-10} torr base pressure) through a load lock (5 x 10^{-8} torr base pressure) and resistively heated for 180 s at the growth temperature to desorb the native oxide layer. The heating assembly consisted of a tungsten wire coil surrounded by a SiC-coated graphite shell. Layers of W and Mo heat shielding were placed on the inside of this shell to reflect heat onto the backside of the sample. This heater is capable of long-term operation at constant temperatures (±3°C) to 1600 K, as measured with an infrared thermometer.

The introduction of ethylene and disilane (both 99.99% purity) into the growth chamber were controlled by a differential pressure transducer which measured the pressure drop across a flow element of essentially constant conductance [7,8]. The pressure drop across the element, ΔP, and the conductance of the element, C, were then converted to flow rate, Q, using the relation $Q = C\Delta P$. A servo-driven leak valve was used to stabilize the flow at the desired level via a feedback loop. In this manner the flow rate of a gaseous species (and

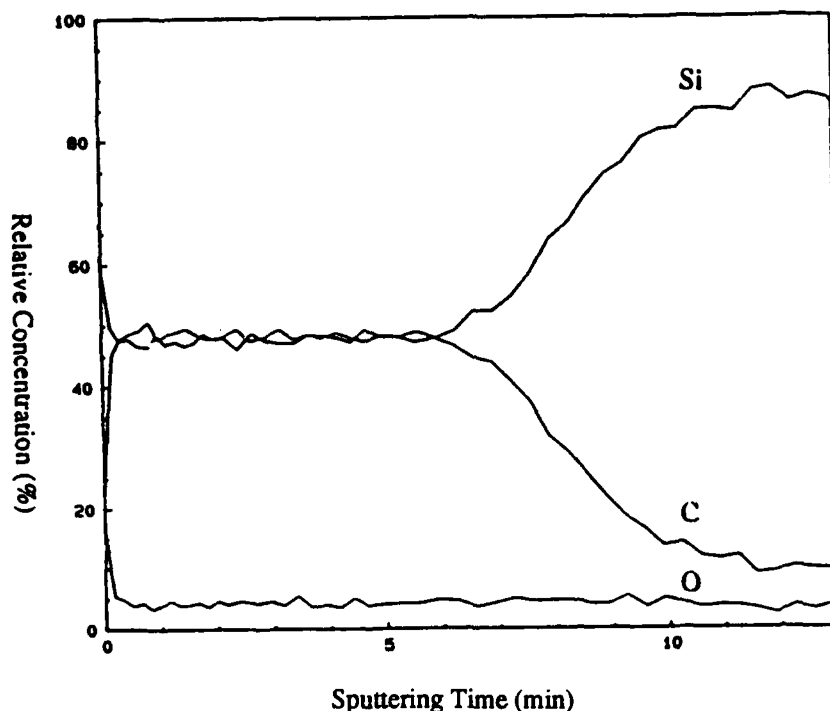

Figure 2. Auger depth profile of sample grown at 1075°C

consequently species flux) were known and controlled at flow rates substantially less than 1 sccm.

Growth conditions used in this study were as follows: temperature, 1298-1498 K; pressure, 4-6 x 10^{-5} torr; Si_2H_6 flow rate, 0.40-2.0 sccm; C_2H_4 flow rate, 2.0 sccm; and time, 90 min. The resulting films were 30-50 nm in thickness. The chemical composition and depth profile of each sample were obtained using a scanning Auger microprobe. Samples which showed a 1:1 Si to C ratio from the Auger results were examined using an optical microscope and a field-emission scanning electron microscope (SEM) to observe surface morphology. Reflection high-energy electron diffraction (RHEED) was used after growth was completed to determine the crystalline quality of the SiC surface. Cross-sectional transmission electron microscopy (XTEM) also was employed to analyze representative β-SiC films. XTEM sample preparation procedures were similar to those used in Ref. 9.

3. Results and Discussion

Auger spectra from the surface of each sample showed the presence of an oxide from atmospheric exposure between growth and analysis. However, the underlying films in most samples were stoichiometric SiC. Figure 2 shows the Auger depth profile adjusted for differences in Auger yield of Si and C from a sample grown directly on off-axis (100) Si at 1298 K using 2.0 sccm C_2H_4 and 0.4

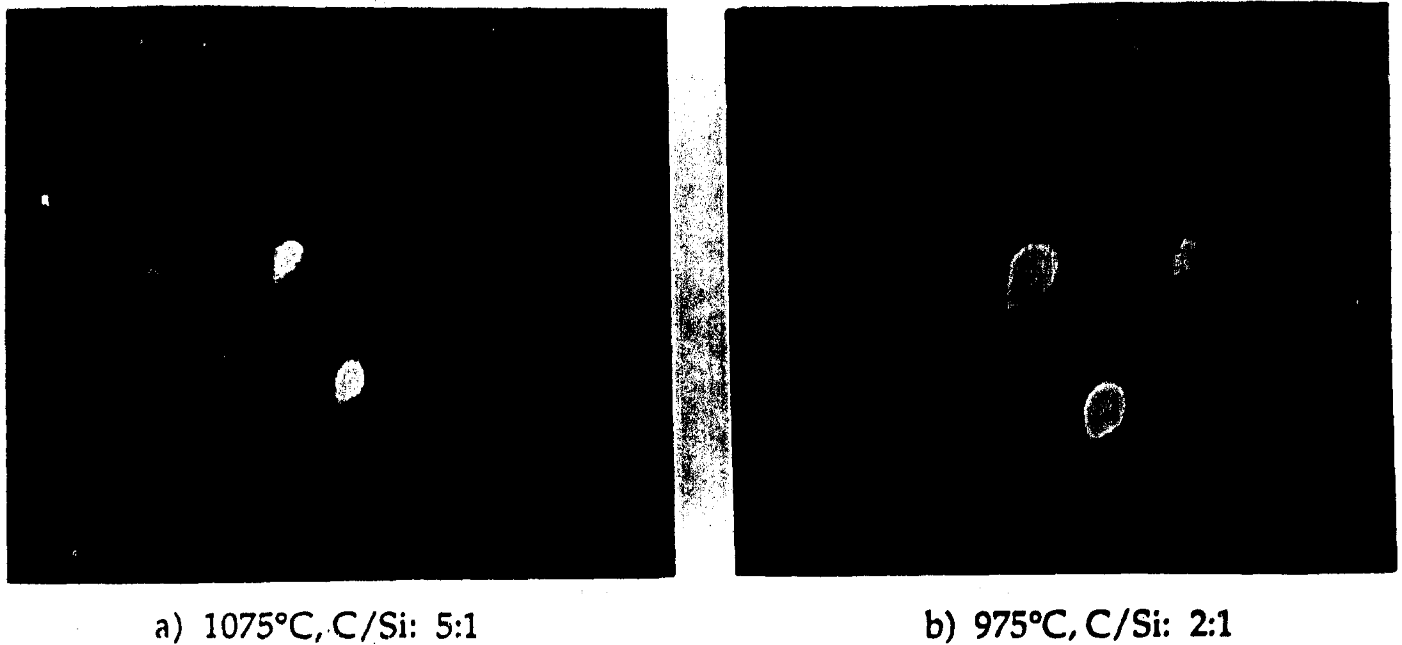

a) 1075°C, C/Si: 5:1   b) 975°C, C/Si: 2:1

Figure 3. RHEED of β-SiC films on Si (100) substrates

sccm Si_2H_6 for 90 min. The results indicate essentially a 1:1 SiC ratio. The oxygen profile within the film is representative of the background level for this Auger system. A monocrystalline β-SiC film previously grown in our laboratory on (100) Si using CVD showed a depth profile nearly identical to that found in the SiC film shown in the figure. Figure 3(a) shows the RHEED pattern ([110] beam azimuth) of the same sample used to obtain the Auger profile of Fig. 2. The RHEED pattern of a sample grown for 90 min on off-axis (100) Si at 1248 K with 2.0 sccm C_2H_4 and 1.0 sccm Si_2H_6 is shown in Fig 3(b). Both samples were monocrystalline β-SiC and were of similar crystalline quality. Twin spots were detected in the RHEED micrographs.

Auger results indicated that only certain C_2H_4:Si_2H_6 flow ratio and temperature combinations resulted in growth of single phase SiC. For example, Si-rich films were obtained for 2.0 sccm C_2H_4 and 0.4 sccm Si_2H_6 at 1248 K and at 1348 K. However, at 1298 K, the film grown using these flow rates was stoichiometric SiC. Films grown using 2.0 sccm C_2H_4 and 2.0 sccm Si_2H_6 were also Si-rich at 1348 K, but were stoichometric at 1298 and 1248 K. Films grown using 2.0 sccm C_2H_4 and 1.0 sccm Si_2H_6 were nominally 1:1 SiC over the entire temperature range investigated. The reasons for these variations are being studied.

Films which were monocrystalline SiC appeared smooth to the naked eye and had a yellowish tinge. Figure 4 is an SEM micrograph of the surface of a sample grown at 1298 K using 2.0 sccm C_2H_4 and 0.4 sccm Si_2H_6. At this

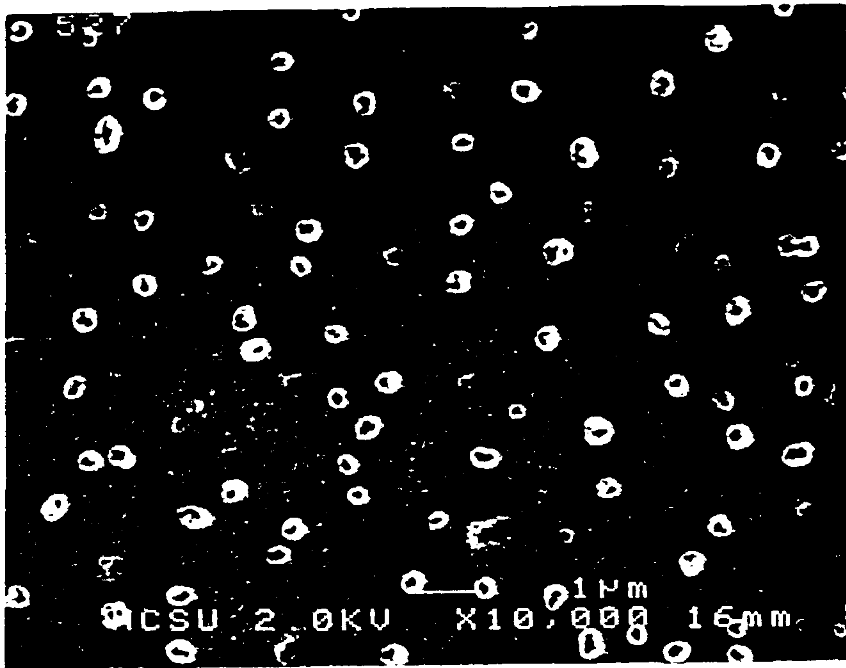

Figure 4. SEM micrograph of β-SiC grown at 1075°C showing preferential growth on pitted regions

resolution, the surface continued to appear fairly smooth except for the presence of pitted regions on the SiC surface. Many of these pits, which are believed to be pyramidal and bounded by {111} planes [10], have preferential growth on their edges. Similar examination of other samples with differing gas source ratios and temperatures provided evidence that growth on the pit edges eventually converges above the center of the pit, forming a hillock above each pit [11].

Transmission electron microscopy (TEM) was used to evaluate the structural quality of the films. Figure 5 shows a high-resolution cross-sectional micrograph and corresponding (110) electron diffraction patterns of both the β-SiC film grown at 1298 K for 90 min and the Si substrate. Both the SiC/Si interface and the SiC surface were fairly rough. The region at the substrate/film interface appears to be amorphous in the micrograph; this is believed to be caused by damage from the ion milling used as part of the TEM sample preparation procedure [1]. A high concentration of defects, namely [111] microtwins and misfit dislocations, are readily visible in the SiC film in the figure. An epitaxial relationship between the SiC film and the Si substrate can clearly be seen in the figure.

Growth thicknesses were estimated from Auger depth profiles and correlated with thicknesses obtained for samples examined using XTEM. The average values were 30-50 nm for 90 min of growth. Experiments designed to increase the SiC growth rate by changing source flow rates or using more reactive, carbon-bearing species are currently in progress.

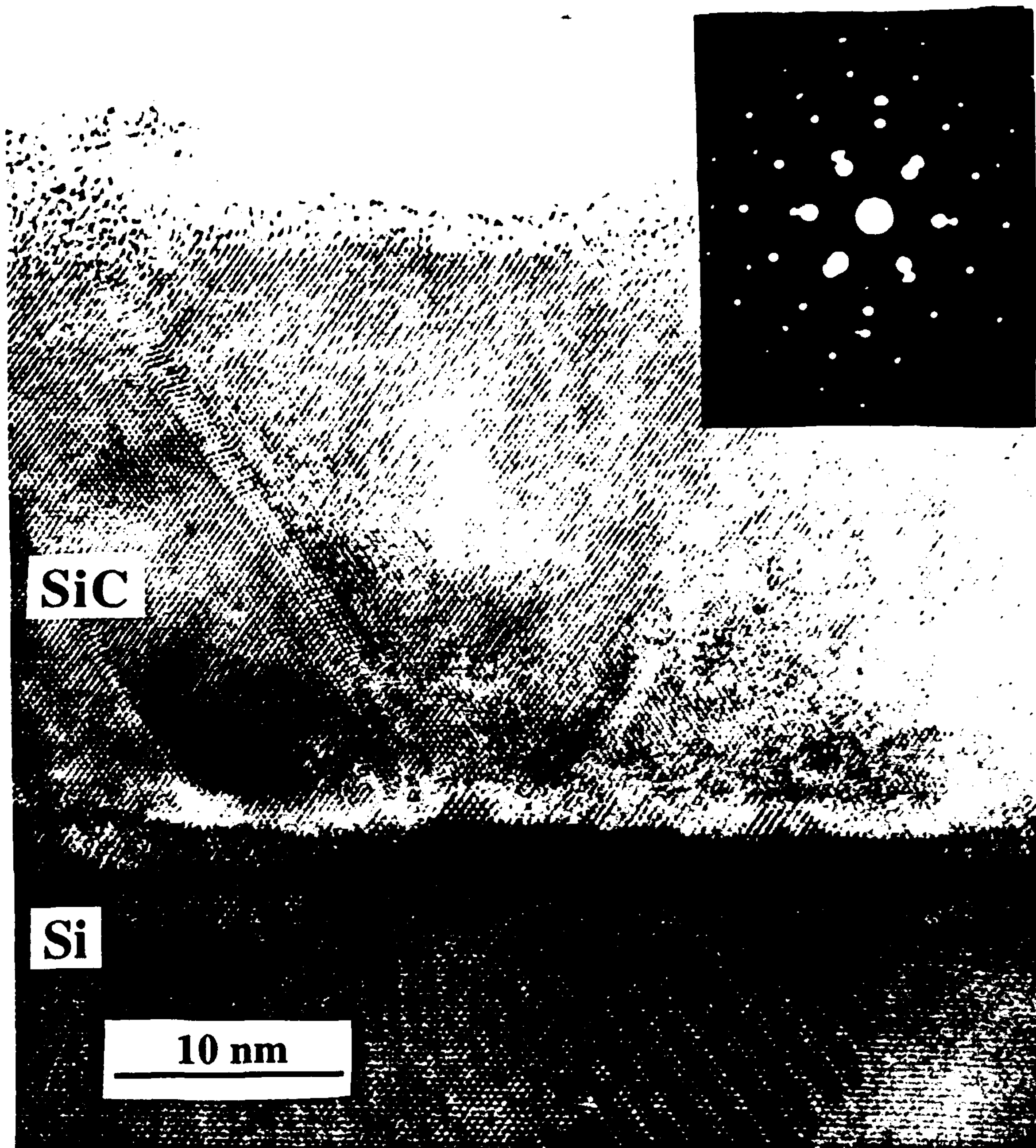

Figure 5: Cross-sectional TEM micrograph of SiC/Si sample grown at 1075°C with inset of selected area diffraction pattern of the SiC film and Si (100) substrate

4. Conclusions

Monocrystalline β-SiC films were grown by GSMBE on off-axis Si (100) substrates using Si_2H_6 and C_2H_4 at temperatures as low as 1248 K. This temperature is much lower than that typically used for SiC CVD growth. Films appeared smooth and specular to the naked eye, but {111} pyramidal growth pits were present on

the film surface. Preferential growth on the pit edges under certain growth conditions was also observed. Cross-sectional TEM analysis of selected SiC films showed the presence of [111] microtwins and visually confirmed the epitaxial relationship between the film and the Si substrate.

Acknowledgements

The authors wish to thank Z. Sitar and M. J. Paisley for the RHEED analysis and S. H. Rogers for the Auger analysis. This research was supported by the Office of Naval Research (Grant No. N00014-88-K-0341/P00002).

References

1. H. J. Kim, R. F. Davis, X. B. Cox, and R. W. Linton, J. Electrochem. Soc. **134**, 2269 (1987)
2. S. Motoyama and S. Kaneda, Appl. Phys. Lett. **54**, 242 (1989).
3. T. Fuyuki, M. Nakayama, T. Yoshinobu, H. Shiomi, and H. Matsunami, J. Cryst. Growth **95**, 461 (1989).
4. T. Sugii, T. Aoyama, and T. Ito, J. Electrochem. Soc. **137**, 989 (1990).
5. K. Shibahara, S. Nishino, and H. Matsunami, Appl Phys. Lett **50**, 1888 (1987).
6. J. A. Powell, L. G. Matus, M. A. Kuczmarski, C. M. Chorey, T. T. Cheng, and P. Pirouz, Appl. Phys. Lett. **51**, 823 (1987).
7. R. A. Kiesling, J. J. Sullivan, and D. J. Santeler, J. Vac. Sci. Technol. **15**, 771 (1978).
8. H. Ishikawa, H. Ando, K. Kondo, A. Sandhu, E. Miyauchi, T. Fujii, and S. Hiyamizu, J. Vac. Sci. Technol. A **8**, 805 (1990).
9. C. H. Carter, Jr., R. F. Davis, and S. R. Nutt, J. Mater. Res. **1**, 811 (1986).
10. A. Addamiano and J. A. Sprague, Appl. Phys. Lett. **44**, 525 (1983).
11. L. B. Rowland et al., to be published.

IV. Gas-Source Molecular Beam Epitaxy of Al-Doped β-SiC on 6H-SiC

A. Introduction

Beta SiC, the lone zincblende (cubic) polytype in the Si-C system, is a candidate material for use in specialized electronic applications because of its attractive physical and electronic properties. These characteristics include wide band gap (2.2 eV at 300K) [1], high breakdown electric field (2.5×10^6 V/cm) [2], high thermal conductivity (3.9 W/cm °C) [3], high melting point (3103K at 30 atm) [4], high saturated drift velocity (2×10^7 m/s) [5, 6], and small dielectric constant (9.7), such as 6H-SiC [7], β-SiC is preferable to hexagonal SiC for most device applications.

Most β-SiC thin film growth to date has been performed on Si substrates. Large-area, crack-free, and relatively thick (up to 30 μm) epitaxial β-SiC thin films have been grown on Si (100) by exposing the Si substrate to C-bearing gaseous species prior to further SiC growth [8-10]. However, these films exhibited large numbers of line and planar defects due to large lattice and thermal mismatches between SiC and Si. One particular type of planar defect, the inversion domain boundary (IDB), was eliminated with the use of Si (100) substrates cut 2°-4° toward [011] [11-13]. Growth on Si substrates has allowed understanding of the SiC growth processes and device development to occur, but the large thermal and lattice mismatches between SiC and Si hamper further development using Si substrates. As a result, considerable effort has been exerted to develop methods for growth of SiC single crystal substrates for homoepitaxial growth of SiC thin films.

Since the 1950's, monocrystalline single crystals of α(6H)-SiC have been formed using the Lely sublimation process [14]. However, since nucleation was uncontrolled using this process, material having a single polytype and uniform doping concentration was difficult. Alpha-SiC single crystals inadvertently formed during the industrial Acheson process have also been used as substrates for SiC growth. However, neither these crystals nor those formed using the Lely process are large enough for practical device applications. Recently, through the use of a seeded sublimation-growth process, boules of single polytype 6H-SiC of > 1 inch diameter with much higher quality than that obtained using the Lely process have been grown. The use of single crystals of the 6H polytype cut from these boules has given a significant boost to SiC device development.

The use of nominally on-axis α(6H)-SiC substrates has usually resulted in growth of β-SiC (111) films [15]. These films have typically had much lower defect densities than those grown on Si substrates. The major defects present in β-SiC/6H-SiC films have been double positioning boundaries (DPB) [16]. Despite the presence of DPBs, the resultant material was of sufficient quality to further device development of SiC. The use of off-axis 6H-SiC (0001)

substrates has resulted in growth of high-quality monocrystalline 6H-SiC layers with very low defect densities [17].

In addition, the use of more advanced deposition techniques, such as molecular beam epitaxy (MBE), has been reported for SiC film deposition. The employment of this technique allows for the reduction in the growth temperature from the 1400-1500°C range which is used in CVD on 6H-SiC substrates. Silicon and C electron-beam sources have been used to epitaxially deposit SiC on 6H-SiC (0001) at a temperature of 1150°C [18]. Ion-beam deposition of epitaxial β-SiC on 6H-SiC has also been obtained at the temperature of 750°C using mass-separated ion beams of $^{30}Si^+$ and $^{13}C^+$ [19]. In order to reduce the temperature of deposition, decrease defect density, and improve electrical characteristics of doped and undoped SiC films, a gas-source molecular beam epitaxy (GSMBE) system has been designed, fabricated, and commissioned for this purpose at NCSU for the research in this contract. In this report, the preliminary results of the epitaxial growth and doping of β-SiC (111) films on 6H-SiC (0001) substrates using this system are presented.

B. Experimental Details

These films were grown on the Si face of 6H-SiC (0001) substrates provided by Cree Research, Inc. The substrates were nominally on-axis (± 1° off (0001)), as determined by X-ray diffraction using the Laue back-reflection method. Films were grown using the MBE/ALE system detailed in previous reports. Readers are referred to these reports for a description and schematics of the system. The material sources used include the gases of Si_2H_6 for silicon, C_2H_4 for carbon and solid Al for the p-type dopant. The last material was evaporated from a standard Knudsen-cell. The 6H-SiC substrates were chemically cleaned prior to growth using a BOE etch at room temperature for 5 min, followed by a DI water rinse for 2 min. This limited cleaning process was used to preserve a sputtered carbon layer present on the back of the wafer as an aid in temperature measurement.

In order to desorb hydrocarbon and oxide layers from the SiC surface, the sample was heated under vacuum to 1250°C for 5 min prior to growth. An Al-doped layer of β-SiC was formed by GSMBE on the converted layer using these conditions: Si_2H_6 flow, 0.5 sccm; C_2H_4 flow, 1.0 sccm; sample temperature, 1250°C; Al source temperature, 960°C; and time, 100 min. The system base pressure was less than 1×10^{-9} torr; pressures during the SiC GSMBE growth typically reached 3×10^{-5} torr.

The surface morphology of the resultant films was examined using optical microscopy and field-emission scanning electron microscopy (SEM). The change of atomic concentration of Al vs. depth was determined using secondary ion mass spectrometry (SIMS). A Cameca IMS-3f ion microprobe was used for this purpose. Mass-filtered O_2^+ at 50 keV was used as the primary ion with a beam raster size of 250 μm. The atomic concentration of Al at each point in

the SIMS profile was obtained by multiplying a conversion factor by the value of the Al/Si count ratio at that point. The conversion factor was determined from the product of the Al/Si count ratio of an Al-implanted profile standard and the theoretically calculated atomic concentration at the peak of this standard. High-resolution transmission electron microscopy (HRTEM) was employed to determine the defects and crystalline structure present in the film as well as examining the film/interface region. An Akashi EM-002B HRTEM was used for this purpose.

C. Results

An SEM micrograph of a heavily Al-doped film grown on SiC (0001) is shown in Figure 1. The surface of the film is fairly smooth, though the existence of small platelets on the surface can be seen as areas of lighter contrast in the micrograph. In the research reported by other investigators [15], optical microscopy normally has revealed a mosaic structure consisting of what appeared to be steps and ledges on the β-SiC film on the α-SiC substrate. However, an examination of the film grown in the present research using Nomarski optical microscopy found only occasional areas with this mosaic pattern. The steps and ledges typically seen result from double positioning boundaries, which result when two adjacent β-SiC (111) nuclei form rotated 60° to each other about the <111> axis [16]. Over the bulk of this film, very few of these DPBs could be found using Nomarski optical microscopy or SEM. It is unclear whether the lack of appearance of DPBs is due to the fact that the film is quite thin (100 nm) or that the nuclei are very small, or the presence of Al has a positive effect or that low temperature MBE growth is effective in eliminating these defects. Plan view TEM and X-ray topography has been used in the past to elucidate these defects, and these techniques will be attempted to determine the presence of DPBs.

A plot of Al atomic concentration vs. depth for this sample is shown in Figure 2. The substrate should have a much lower concentration of Al than the film which was intentionally heavily doped. The peak concentration of Al is high (5×10^{20} cm^{-3}). However, the Al concentration drops rapidly with depth. It is believed that the small hump seen at a sample depth of about 100 nm denotes the interface between the β-SiC film and the 6H-SiC substrate. There should be some small amount of strain at this interface (even though the substrate and film are both SiC). This strain is primarily due to the different doping levels and impurity concentrations of the film from the substrate, and also the different crystal structures of the two SiC polytypes. This interfacial strain energy, though small, would enable the formation of lower-energy sites for impurity species such as Al. This decrease in lattice strain energy resulting from the incorporation of Al near the interface would encourage migration of this species to the interface during deposition.

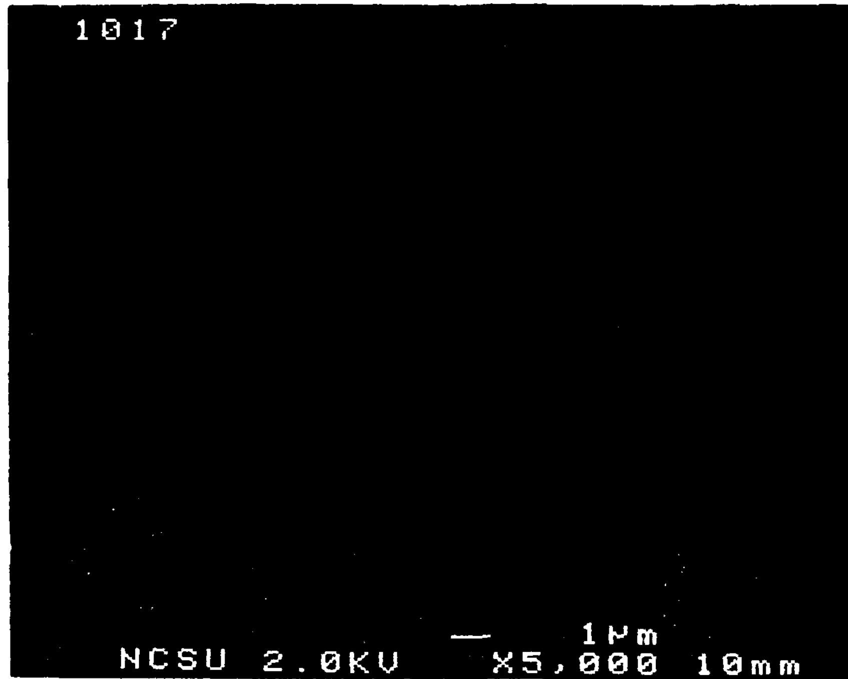

Figure 1: Scanning electron microscopy micrograph of the surface morphology of a heavily Al-doped β-SiC film by scanning electron microscopy.

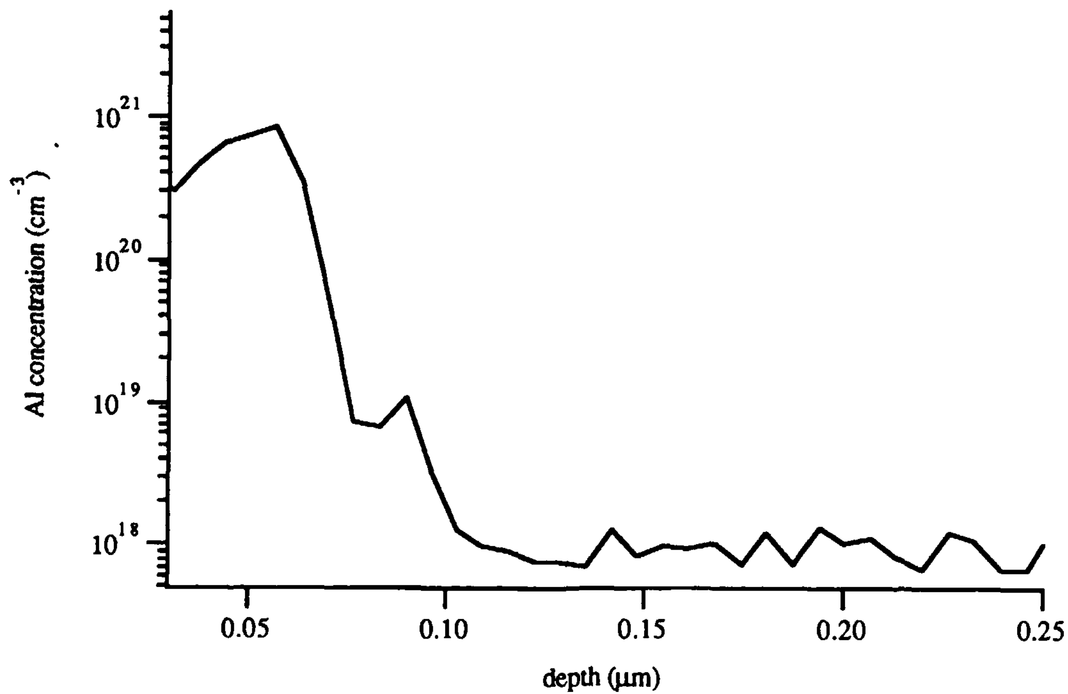

Figure 2: Atomic concentration vs. depth of Al in β-SiC film deposited on α(6H)-SiC substrate.

Figure 3 is a cross-sectional HRTEM micrograph of a portion of the film and the β-SiC/6H-SiC interface. The substrate is oriented so that the [1120] direction of the 6H-SiC substrate is perpendicular to the plane of the image. It was deduced that the 6H-SiC substrate used in this experiment was almost exactly in the (0001) orientation due to the lack of steps at the top of the 6H-SiC substrate layer. From the lattice images of the film, the grown layer is deduced to be cubic and in the (111) orientation. Several (111) stacking faults can be seen in the micrograph (where the film appears to become 6H-SiC for a few layers). A selected area diffraction (SAD) pattern of the film and the substrate is shown in Figure 4. Diffraction spots from both the 6H-SiC substrate and the β-SiC layer can be seen. The epitaxial relationship between the substrate and the β-SiC film can also be observed both from the micrograph and the corresponding SAD pattern.

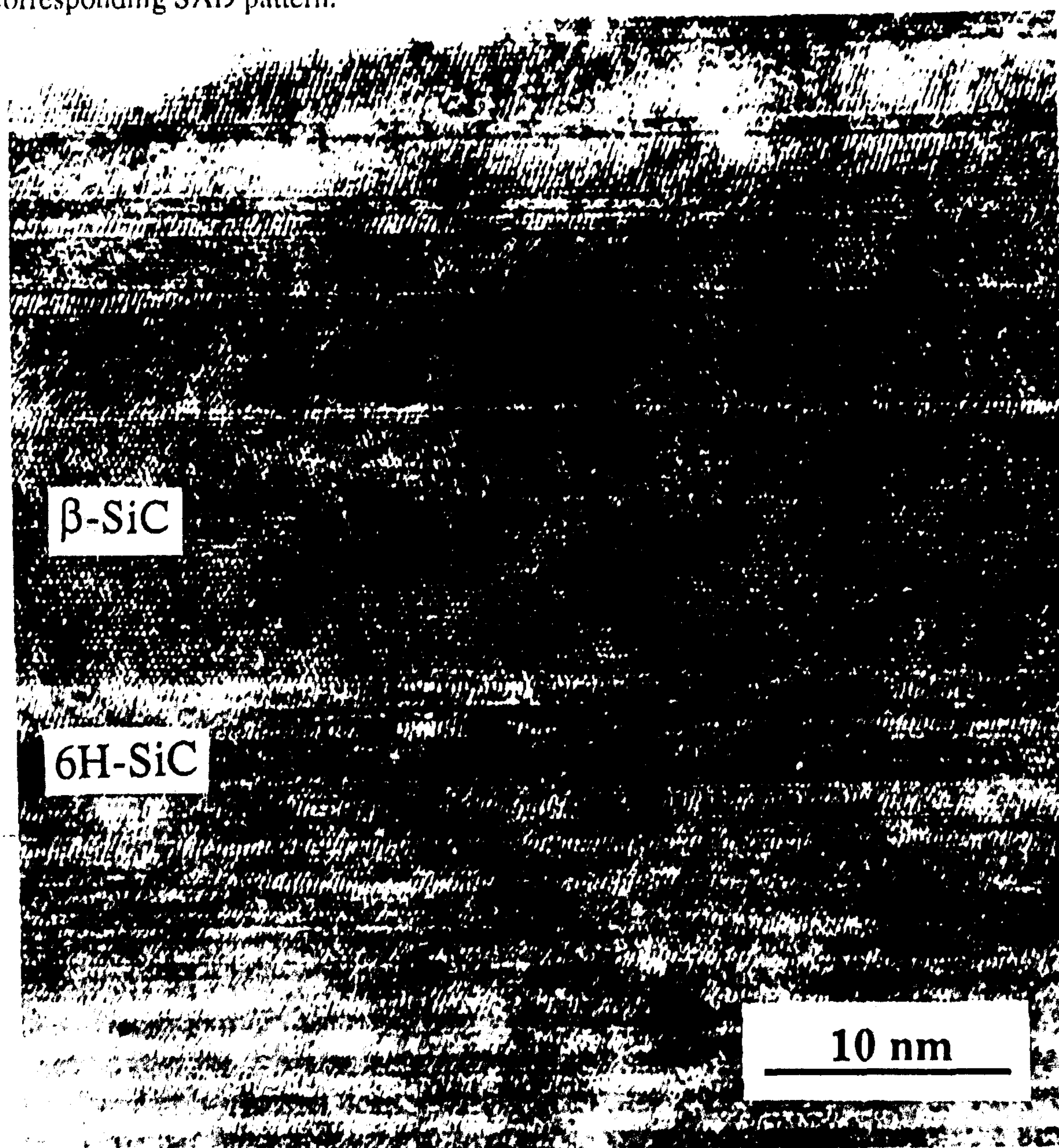

Figure 3: Cross-sectional HRTEM image of β-SiC film and 6H-SiC substrate.

Best Available Copy

Figure 4: Selected area diffraction pattern of β-SiC film and 6H-SiC substrate.

D. Discussion

The surface morphology of the as-grown film is fairly smooth, and appears to be relatively free of DPBs, as compared to conventional CVD growth. Several researchers [17-21] have suggested that variations in surface treatment prior to growth can change the density of or virtually eliminate DPBs formed on the resultant film. Variations in cleaning method have been shown to change DPB density, with the lowest DPB density obtained on the as-received wafers in one study [20]. The effects of annealing in H_2 and growth of thin Si and C layers prior to β-SiC growth on 6H-SiC substrates have also been examined, with most promising results obtained using conversion of a Si pre-growth layer to SiC followed by SiC film growth [21]. In any case, pre-growth treatment of the substrate has been shown to affect DPB density. It is conceivable that DPB formation could be arrested using MBE, if the initial several layers formed were somehow continuous. The level of control using MBE is much greater than with CVD, and this greater control could allow for layer growth on 6H-SiC substrates. Examining the films during growth using *in situ* reflection high-energy electron diffraction (RHEED), as is planned in the near future, should prove conclusive as far as determining whether layer growth is present in the first few monolayers of β-SiC. In addition, as mentioned previously, examination of the MBE-grown films using other methods such as plan-view TEM is necessary to determine whether DPBs actually are present.

The β-SiC film discussed in this report is heavily doped with Al, with a peak concentration of 7×10^{20} cm^{-3}. A value of concentration this high is suspect, and as a result, attempts to

duplicate this result are in process. I-V characteristics taken without a rectifying contact indicate that this sample is p-type. Electrical measurements (I-V and C-V) on this sample are being conducted in order to determine both carrier concentration in the layer as well as characterize the p-type β-SiC/n-type 6H-SiC p-n junction. A high concentration of Al may help to explain the presence of <111> stacking faults seen in Figure 3. The concentration of Al in this film, if the SIMS data is correct, would produce large amounts of strain in the film because of the larger size of the Al atom in a tetrahedral bonding configuration. This strain could induce the formation of these stacking faults as a way of alleviating it. Double crystal X-ray diffraction could prove useful in determining the amount of strain present.

E. Conclusions

Gas source MBE growth of heavily Al-doped epitaxial layers of β-SiC (111) on 6H-SiC (0001) has been achieved at 1250°C using C_2H_4 and Si_2H_6 as source gases. This growth temperature is 250°C lower than that typically used in CVD. High-resolution TEM showed a coherent interface between the film and substrate and the presence of [111] stacking faults. The latter occurred periodically in the β-SiC film. These stacking faults may prove to be due to strain induced by the large concentration of Al present in the film. Surface morphological examination of films using SEM and optical microscopy showed an apparent lack of DPB formation. Further characterization is necessary to determine whether or not DPBs exist in these films. SIMS analysis suggested the presence of a high concentration of Al in these films. Electrical measurements will be conducted in the near future.

F. Future Work

Films of both β-SiC and 6H-SiC will be grown on 6H-SiC (0001) substrates. Al-doped films will be grown to determine the ratio of atomic concentration to carrier concentration. In addition, undoped β- and 6H-SiC will be grown to determine background concentrations of impurity species such as N and residual carrier concentrations. P-n junctions grown using this system will be electrically characterized and leakage currents and diode ideality factors obtained.

Growth on RF-sputtered SiC layers on Si cut 3.5° off (100) will also be attempted. This approach will be tried in order to potentially prevent the formation of <111> pits in the Si substrate (these pits are mentioned in the previous section) and to produce very flat surfaces. If these layers are successful in serving as a template for smooth epitaxial β-SiC films, then electrical measurements on these films will be performed as well.

G. References

1. H. P. Philipp and E. A. Taft, in *Silicon Carbide, A High Temperature Semiconductor*, edited by J. R. O'Connor and J. Smiltens (Pergamon, New York, 1960), p. 371.

2. W. von Muench and I. Pfaffender, J. Appl. Phys. **48**, 4831 (1977).
3. E. A. Bergemeister, W. von Muench, and E. Pettenpaul, J. Appl. Phys. **50**, 5790 (1974).
4. R. I. Skace and G. A. Slack, in *Silicon Carbide, A High Temperature Semiconductor*, edited by J. R. O'Connor and J. Smiltens (Pergamon, New York, 1960), p. 24.
5. W. von Muench and E. Pettenpaul, J. Appl. Phys. **48**, 4823 (1977).
6. P. Das and K. Ferry, Solid State Electronics, **19**, 851 (1976).
7. S. Nishino, Y. Hazuki, H. Matsunami, and T. Tanaka, J. Electrochem Soc. **127**, 2674 (1980).
8. S. Nishino, J. A. Powell, and H. A. Will, Appl. Phys. Lett. **42**, 460 (1983).
9. K. Sasaki, E. Sakuma, S. Misawa, S. Yoshida, and S. Gonda, Appl. Phys. Lett. **45**, 72 (1984).
10. P. Liaw and R. F. Davis, J. Electrochem. Soc. **132**, 642 (1985).
11. K. Shibahara, S. Nishino, and H. Matsunami, J. Cryst. Growth **78**, 538 (1986).
12. J. A. Powell, L. G. Matus, M. A. Kuczmarski, C. M. Chorey, T. T. Cheng, and P. Pirouz, Appl. Phys. Lett. 51, 823 (1987).
13. H. S. Kong, Y. C. Wang, J. T. Glass, and R. F. Davis, J. Mater. Res **3**, 521 (1988).
14. J. A. Lely, Ber. Deut. Keram. Ges. **32**, 229 (1955).
15. H. S. Kong, J. T. Glass, and R. F. Davis, Appl. Phys. Lett. **49**, 1074 (1986).
16. H. S. Kong, B. L. Jiang, J. T. Glass, G. A. Rozgonyi, and K. L. More, J. Appl. Phys. **63**, 2645 (1988).
17. H. S. Kong, J. T. Glass, and R. F. Davis, J. Appl. Phys. **64**, 2672 (1988).
18. S. Kaneda, Y. Sakamoto, T. Mihara, and T. Tanaka, J. Cryst. Growth **81**, 536 (1987).
19. S. P. Withrow, K. L. More, R. A. Zuhr, and T. E. Haynes, Vacuum **39**, 1065 (1990).
20. J. A. Powell, D. J. Larkin, L. G. Matus, W. J. Choyke, J. L. Bradshaw, L. Henderson, M. Yoganathan, J. Yang, and P. Pirouz, Appl. Phys. Lett. **56**, 1353 (1990).
21. Y. C. Wang, M. S. Thesis, North Carolina State University, 1991.

V. INTERFACE CHEMISTRY AND SURFACE MORPHOLOGY IN THE INITIAL STAGES OF GROWTH OF GaN AND AlN ON α-SiC AND SAPPHIRE

A. Introduction

Successful commercialization of infrared and selected visible light-emitting optoelectronic devices simultaneously stimulated research in the wide-bandgap semiconductors for similar devices operational in the blue and ultra-violet regions of the spectrum. Much attention has been given to the III-V nitrides, particularly GaN and AlN, which possess direct bandgaps of 3.45 and 6.28 eV, respectively. Since they form a continuous range of solid solutions [1–3] and also superlattices [4, 5] they are suitable for bandgap engineering in the range of 3.45-6.28 eV.

Single crystal wafers of the nitrides are not available, thus they must be grown heteroepitaxially. Sapphire has been the most commonly used substrate, despite the huge lattice mismatch. The quality of heteroepitaxially grown films depends on two key issues: the lattice mismatch between the substrate and the film and the values of their respective surface energies. Both influence film growth in the very early stages and, as such have a significant influence on the overall quality of the heteroepitaxial films.

Three different growth regimes are clearly distinguished. The first one is layer-by-layer (or two dimensional) growth, in which the material is deposited in sequential monolayers of coverage. This type of growth is observed, when the substrate surface energy, σ_S, exceeds the sum of the surface energies of the overgrowth, σ_O, and the interfacial energy, σ_i (i.e. $\sigma_S \geq \sigma_O + \sigma_i$). In other words, the overgrowth "wets" the substrate. The second regime is Stranski-Krastanov growth in which the first few monolayers completely cover the surface of the substrate, while the subsequent layers form islands of deposited material. This type of growth satisfies the same equation as the layer-by-layer growth, but islanding occurs due to high strain energy which arises due to the lattice mismatch. The third regime is three dimensional growth, in which the material immediately forms islands on the surface. This type of growth occurs when $\sigma_S \leq \sigma_O + \sigma_i$. Figure 1 shows schematic representation of all three regimes.

Surface energies of the III-V nitrides have not been measured. A common theoretical method for covalently bonded materials involves the summation of the energies of the broken bonds per unit area of the surface [6]. However, surface bond energies also cannot be determined accurately. As such, one cannot determine from the theoretical modes of surface energy which substrate would be best suited for the heteroepitaxial growth of a certain material, e.g., GaN or AlN.

Experimental determination of the mode of nucleation and growth of a material on a selected substrate usually consists of several sequences of growth of 0.5 to 1 monolayer

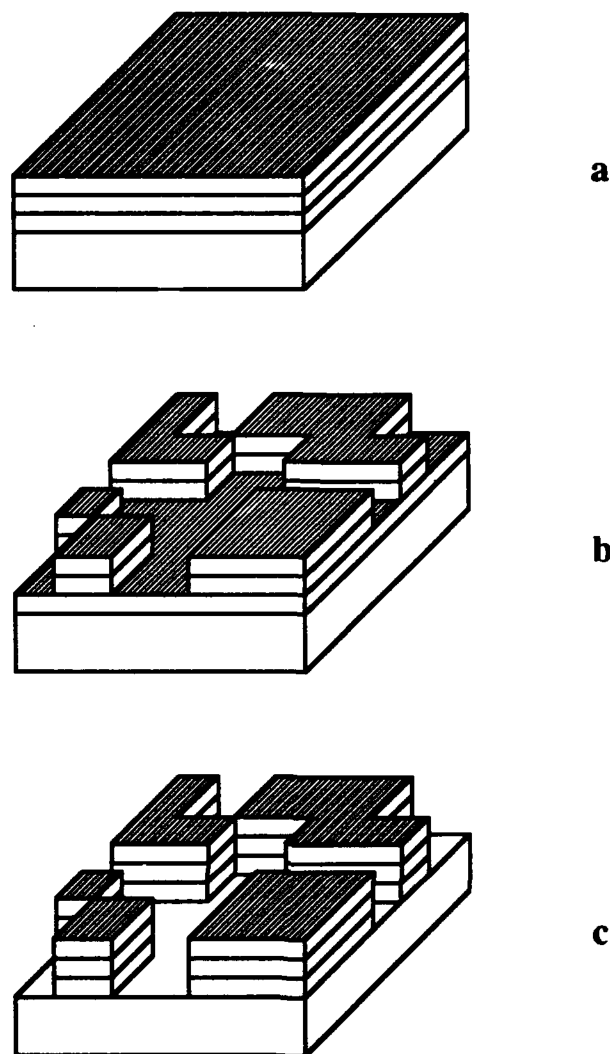

Figure 1. Schematic presentation of the three growth regimes: (a) Layer-by-Layer, (b) Stranski-Krastanov, (c) 3-Dimensional.

of material and analysis of the interface region either by Auger spectroscopy or XPS. The growth steps are repeated until a total of five to ten monolayers have been grown. Such an experiment is built on the fact, that electrons of a well defined energy travel in solids a certain distance without loosing their energy. This distance is called the escape depth. When they pass through a material, the flux of these electrons decreases exponentially. Since low energy electrons (a few 100 eV) have a very short escape depth (usually in the order of a few monolayers), they are a sensitive measuring tool for the characterization of very thin layers. If the substrate is excited with high energy electrons (as in Auger studies) or photons (XPS studies) which easily penetrate the grown film well beyond the escape region for characteristic electrons, one can consider the substrate as a source of an electron flux I_0. If a film is deposited in small steps, the electron flux of characteristic substrate lines decreases

with the film thickness. The dependence of the electron flux on film thickness can provide information regarding the initial growth morphology. A calculated plot of the decrease of the characteristic substrate XPS peak with film thickness for the three types of growth is shown in Figure 2 [7].

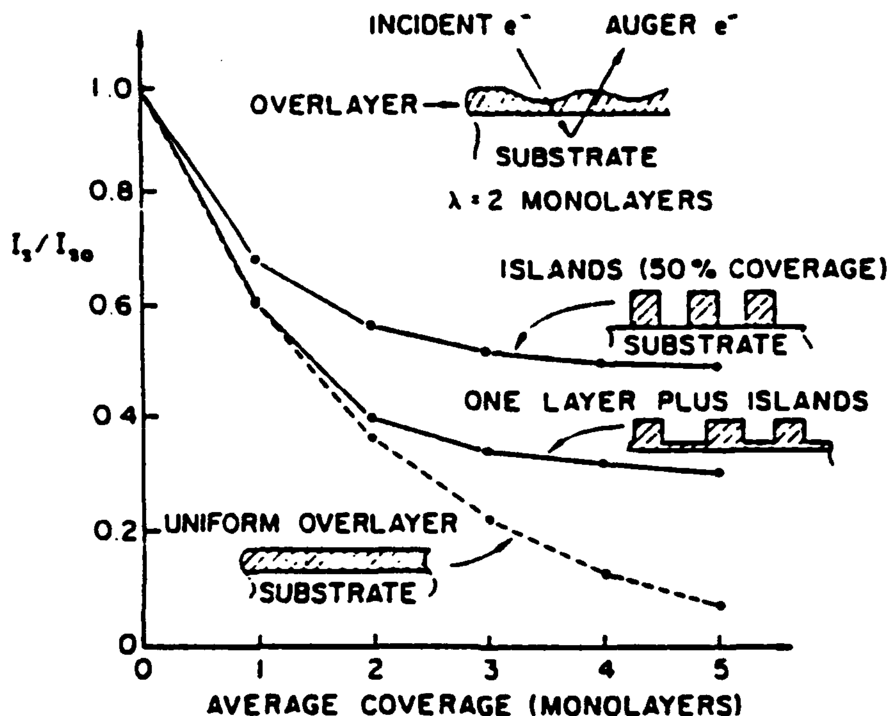

Figure 2. Extinction curves for characteristic substrate electrons as a function of coverage of an overlayer for different types of growth.

B. Experimental Procedures

1. Deposition System

The growth system was a commercial Perkin-Elmer 430 MBE system consisting of three major sections: a load lock (base pressure $\approx 5 \times 10^{-8}$ Torr), a transfer tube connecting the MBE and the analytical chambers (base pressure $\approx 1 \times 10^{-10}$ Torr) which was used to degas the substrates, and the growth chamber (base pressure $\approx 5 \times 10^{-11}$ Torr).

Knudsen effusion cells were used as gallium and aluminum sources. Films of GaN and AlN could not be produced within the experimental conditions of this study using molecular nitrogen. Therefore an ECR plasma source was designed, constructed and commissioned [8] in order to efficiently activate/dissociate molecules of this gas. This unique source has the advantage of fitting inside the 2.25 inch diameter tube of the source flange cryoshroud. Using this design, the source–to–substrate distance was minimized which increased the flux density at the substrate. A similar plasma source was not commercially available at the outset of this

effort. Some important parameters of the ECR source are given in the Table I. Ultra-high-purity nitrogen, further purified by a chemical purifier, was used as the source gas. The flow rate was regulated by a variable UHV compatible leak valve and was normally ≈5 sccm which resulted in a process chamber pressure of 1×10^{-4} Torr.

Table I. Some parameters of the NCSU-ECR nitrogen plasma source.

Parameter	Value
Overall source diameter	57 mm
Plasma diameter	23 mm
Microwave frequency	2.45GHz
Microwave power	0–100 W
Peak magnetic flux	1.05 kG
Nitrogen ion current density at 50 W	
• at the source	≈1 $mAcm^{-2}$
• at the substrate	150–200 μAcm^{-2}
Start pressure	1×10^{-4} Torr
Minimum operation pressure	1×10^{-5} Torr

2. Film Growth

Growth studies were conducted on (0001)-oriented α(6H)-SiC and the basal plane of epitaxial quality sapphire wafers, both of which have a hexagonal structure. All substrates were chemically cleaned to remove organic and metallic contaminants and mounted on a standard 3 inch molybdenum block with indium which provided both good adherence and thermal contact.

The substrates underwent an initial low temperature (≈70°C) outgasing in the load lock followed by slow heating in the transfer tube to a maximum of 700°C with a dwell time of 30 min at this temperature. After cooling, the samples were introduced into the growth chamber and examined by reflection high energy electron diffraction (RHEED) using a 10 kV beam. The resulting RHEED patterns on both the α-SiC and sapphire substrates showed Kikuchi lines, indicative of a good crystalline quality.

Prior to growth, the substrates were heated to the desired deposition temperature and subsequently exposed to a flux of plasma activated nitrogen species for about 5 min. Following the stabilization of temperatures and fluxes, a thin layer of GaN or AlN was grown. The growth conditions are summarized in Table II. After the growth was completed, the gallium or aluminum cell and the substrate were cooled, while the nitrogen source remained active until the substrate temperature was below 400°C. One set of experiments was conducted using photo enhancement, where a 500 W Hg lamp was used to irradiate the

samples during the growth. The XPS results of this study were compared with those described from the unirradiated sample.

Table II. Growth conditions.

Nitrogen pressure	1×10^{-4} Torr
Microwave power	50 W
Gallium temperature	900°C
Aluminum temperature	1120°C
Substrate temperature	600°C
Thickness grown/deposition	0.2 - 0.5 nm
Number of deposition cycles	6 - 7
Total number of monolayers grown	5 - 12

3. XPS Analysis

XPS (X-ray photoelectron spectroscopy) was performed on the cleaned substrates prior to deposition and on the grown films after each deposition step. Samples were transferred from MBE growth chamber to the analytical chamber under UHV conditions. XPS spectra were obtained with a Riber Mg/Al X-ray source and a Riber MAC II cylindrical electron analyzer. Spectral data were acquired by an IBM PC-AT running software developed at NCSU.

For the study of the AlN growth, Mg Kα X-rays (1253.6 eV) were used to obtain spectra. For GaN growth, both the Mg and Al (1486.6 eV) anodes were used. The reason for alternating the X-ray sources for the examination of GaN was due to the fact that the Ga Auger electron emission occupies a large region of the spectrum between 0 and 1000 eV, and covers up certain XPS photoemission peaks of interest. The change of the X-ray energy shifts the Auger emission lines on an intensity vs. binding energy plot for the change in the energy of the X-ray photons, while the positions of the XPS photopeaks remains the same. The effect of changing the energy of X-rays is illustrated in Figure 3. Figure 3(a) is a wide-energy scan survey spectrum of GaN on sapphire obtained with the Mg X-ray anode, showing both substrate and film photopeaks and the Ga_{LMM} Auger emission cluster, which covers about a 250 eV wide band of the spectrum, from 150-400 eV. Figure 3(b) is a similar survey spectrum of GaN on SiC using the Al anode; this spectrum shows that the Ga Auger emission has been shifted by an amount equal to the energy difference between the two sources (233 eV). Owing to the positions of the Ga Auger emission, the Mg anode was used for examining the O_{1s} and N_{1s} photopeaks, while the Al anode was used for examining the C_{1s}, Si_{2s}, Al_{2p} and Ga_{3d} peaks.

For the study of GaN, the Si_{2s} photopeak at 153 eV was used, rather than the more commonly used Si_{2p} peak, again because of interference from Ga emission. The Ga_{3p} peak at

107 eV lies very close to Si_{2p} at 103 eV, and overwhelms the Si_{2p} emission, as the Ga signal increases with the thickness of GaN film. The Si_{2s} peak is also near another Ga photopeak (Ga_{3s} at 160 eV) but is located farther from the nearby Ga peak than the Si_{2p} peak is from its Ga neighbor. No switching of the anodes was necessary for the examination of AlN films. All photo-peaks of interest are well resolved on both substrates with the Mg anode, as can be seen in Figures 4 (a) & (b), which show a broad energy scan of AlN on SiC and sapphire, respectively.

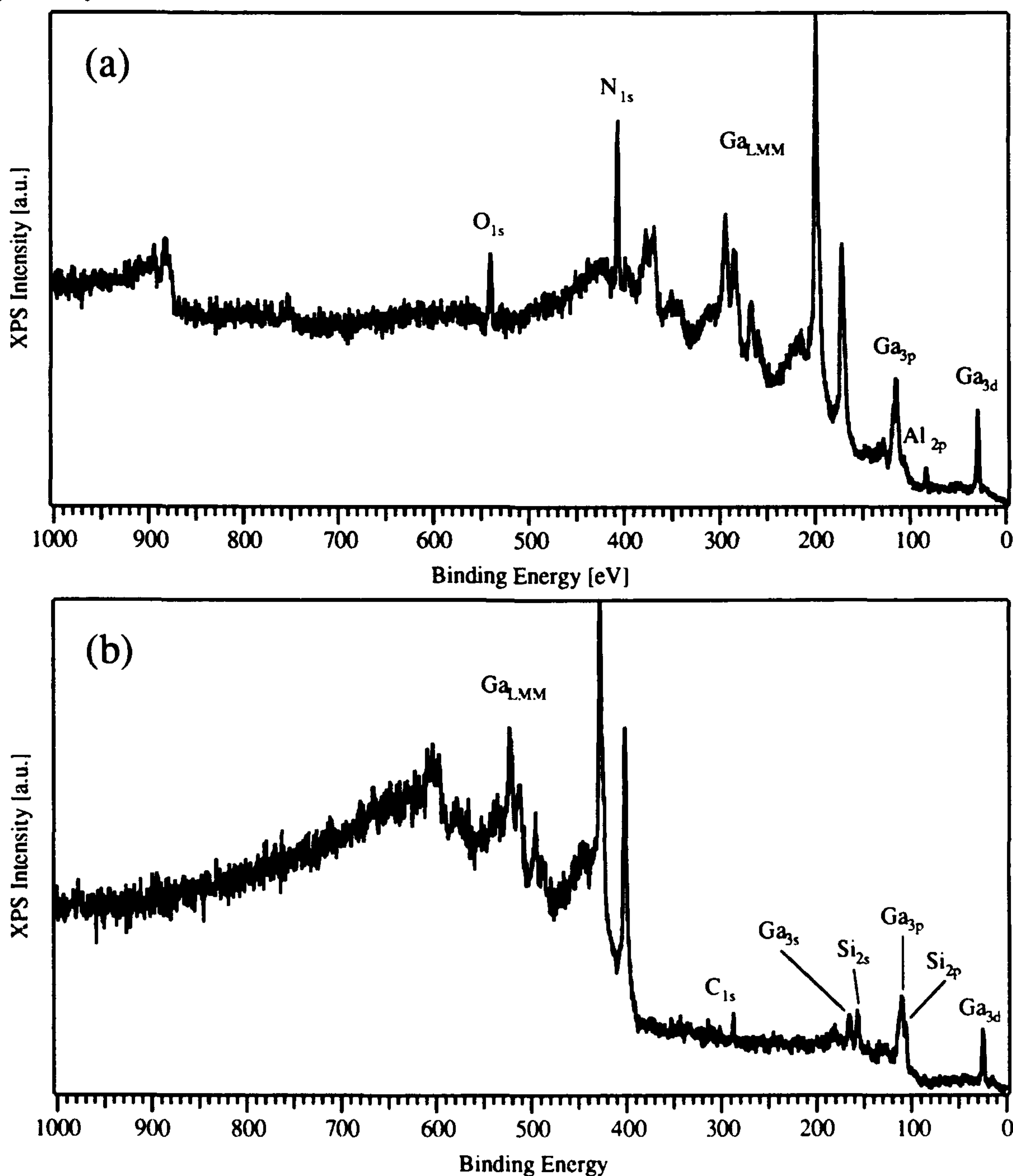

Figure 3. XPS survey spectra of GaN films: (a) Sapphire substrate, Mg X-ray source. (b) SiC substrate, Al X-ray source.

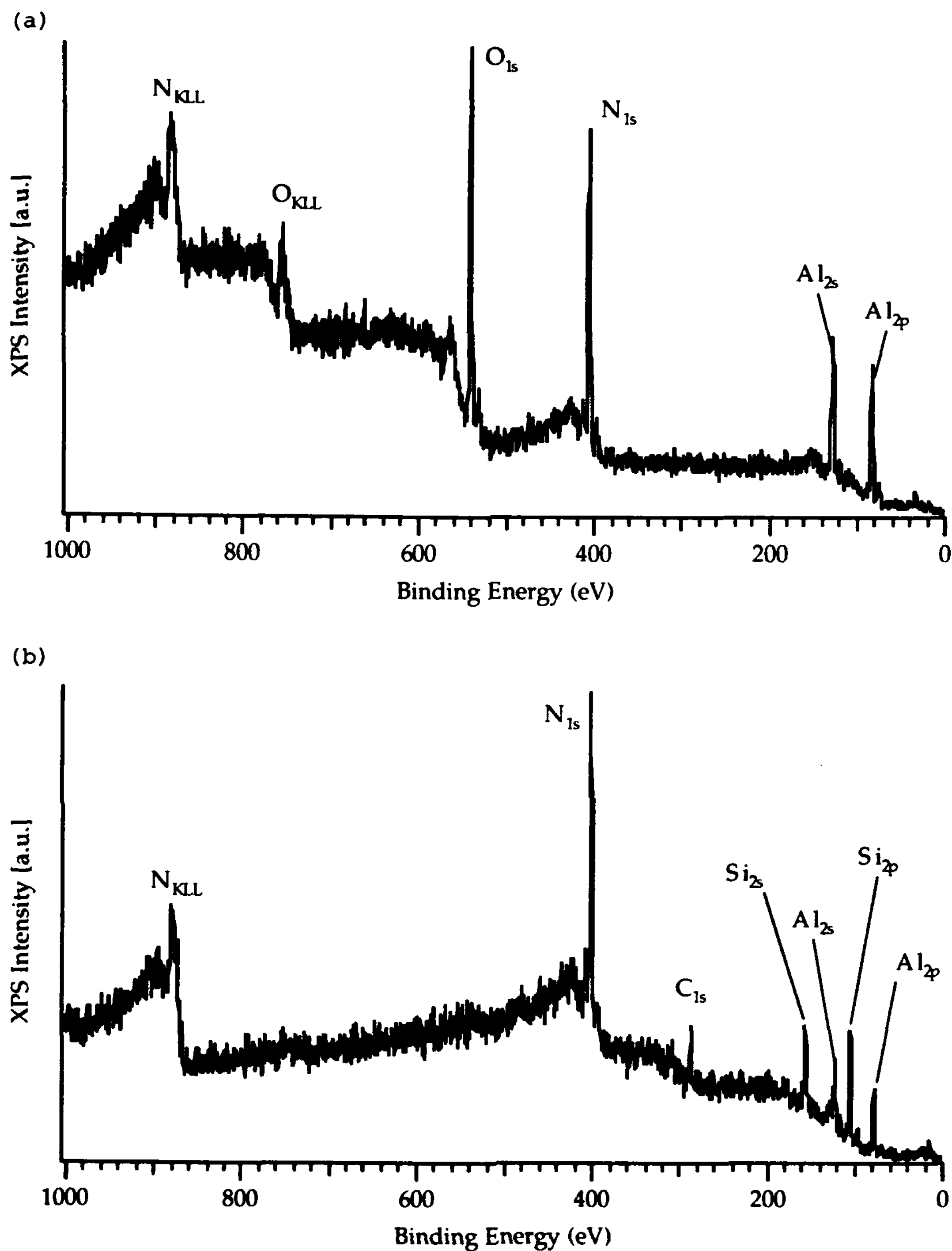

Figure 4. XPS survey spectra of AlN films: (a) Sapphire substrate, (b) SiC substrate. Mg X-ray source was used in both cases.

Electron escape depths were obtained from the universal curve of mean free path of electrons vs. their energy.[7] The escape depth is relatively insensitive to the material traversed by the electrons. Since XPS photoelectrons of C_{1s}, Si_{2s} and O_{1s} have considerably different binding energies, the energies of the escaped electrons differ as well. Since the energy of an escaped electron equals the incident X-ray photon energy minus the electron

binding energy, electrons with higher binding energy acquire less kinetic energy when being excited with the same kind of X-rays. Switching anodes from Mg to Al has an effect on the kinetic energy as well. The escape energies of selected photoelectrons and their respective escape depths are summarized in Table III.

Table III. Photoelectron energies and their escape depths.

	O_{1s}	C_{1s}	Si_{2s}
Photon Energy [eV]	1254 (Mg)	1487 (Al)	1487 (Al)
Binding Energy [eV]	531	283	152
Kinetic Energy [eV]	723	1204	1335
Escape Depth [Å]	12±1	18±1	18±1

Si_{2s} and C_{1s} peak intensities were monitored during the growth on SiC substrates and O_{1s} peak was examined during the growth on sapphire. The areas of the substrate peaks obtained after each deposition were calculated, compared to the areas of the peaks from the virgin substrate, and finally plotted vs. thickness of deposited material. Results were compared with a theoretical curve for layer-by-layer growth.

The binding energy value of each of the XPS photopeaks was referenced to the peak position, which was expected to be the most invariant. This procedure minimizes the effects of the analyzer characteristics and specimen charging. For the films grown on SiC, the C_{1s} peak was set at the typical value for SiC of 283.0 eV[9-11]. The other peaks were referenced to that value. For the films grown on sapphire substrates, the N_{1s} values of 397.0 for GaN [11, 12] and 397.3 for AlN [11, 12] were used as reference positions. For the clean sapphire substrates, prior to deposition, the photopeaks were referenced to the average value for O_{1s} observed during the remainder of the deposition.

C. Results and Discussion

1. Growth Morphology: GaN

Figures 5 and 6 show plots of relative substrate peak intensities vs. film thickness obtained during the growth of GaN both without (Fig. 5) and with (Fig. 6) UV treatment during growth. Both figures also contain theoretical curves representing layer-by-layer growth calculated at two escape depths, 12 (C_{1s},Si_{2s}) and 18 (O_{1s}) Å. The two curves correspond to the growth on SiC and sapphire, respectively.

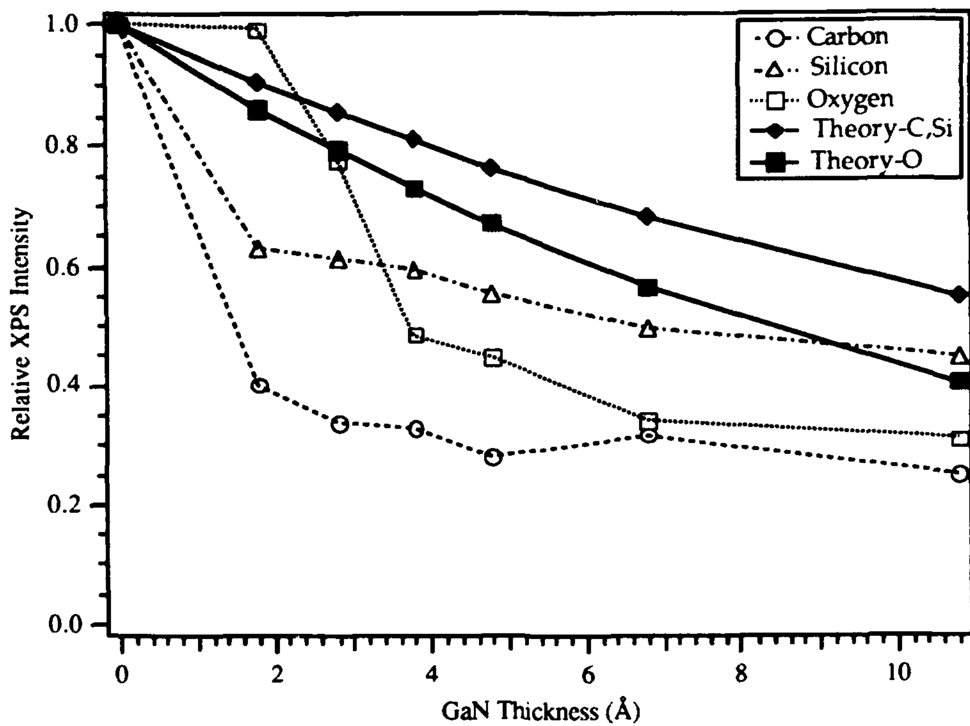

Figure 5. Change of XPS photoelectron intensity during growth of GaN on α(6H)-SiC and sapphire.

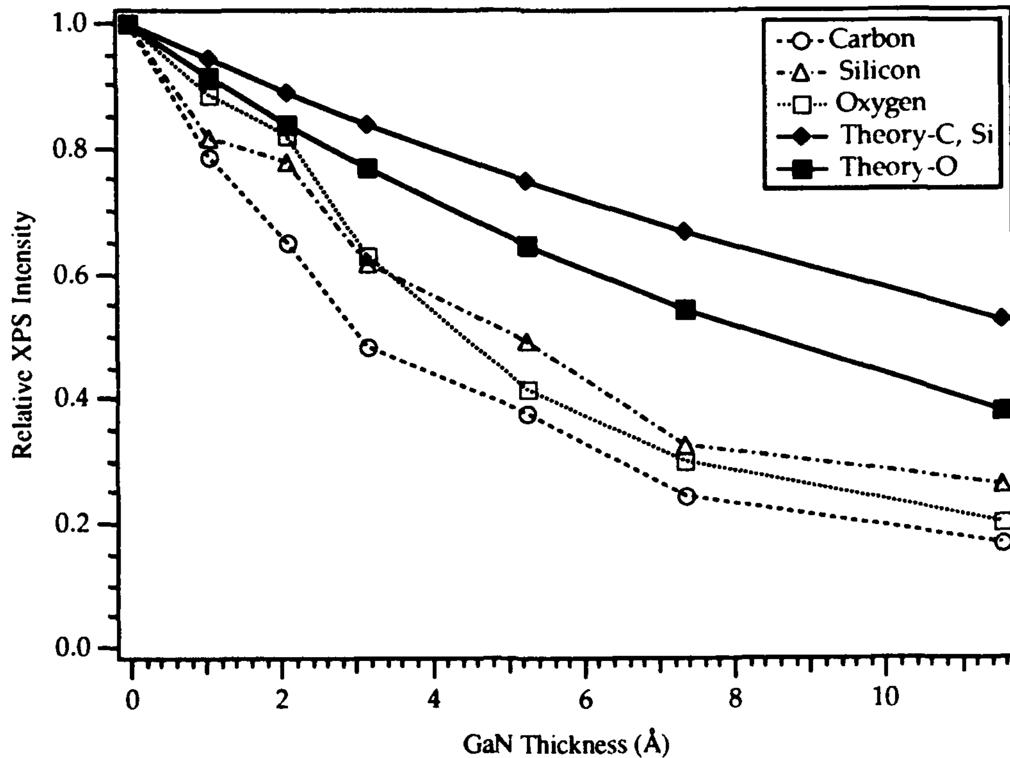

Figure 6. Change of XPS photoelectron intensity during UV-enhanced growth of GaN on α(6H)-SiC and sapphire.

The plots in Figure 5 show that the substrate peak intensity diminishes initially faster for the growth of GaN on SiC than on sapphire (compare O_{1s} to C_{1s} and Si_{2p} signals). This is most likely due both to a faster initial nucleation process on SiC, and to the formation of a thin silicon nitride layer at the interface (see below). This reasoning also agrees with the behavior of the O_{1s} signal. This signal decreases rapidly, once initial nucleation occurs, and with the same slope as the Si_{2p} and C_{1s} signals at the very beginning of the growth. Furthermore, an earlier study in the authors' laboratory of the growth rate of GaN on different substrates did not indicate a substantial difference between the growth rates on SiC and sapphire within experimental conditions. The growth rate was controlled by the Ga arrival rate rather than by any other factors.

Similar behavior for the change in the intensity of the Si_{2s} and C_{1s} photoemission was anticipated, since they originate from the same SiC substrate. However, this was not observed. As shown in Figure 2, the C_{1s} peak intensity shows a faster initial drop and also saturates at a lower value. This can also be explained by the formation of a thin layer of silicon nitride. Since the Si-face of the SiC substrates was used, a silicon nitride layer formed on the surface during exposure to the reactive N species prior to film deposition. This resulted in burying the carbon layer more deeply under the Si. The difference in the initial intensity drop approximately corresponds to the formation of one monolayer of silicon nitride.

All three curves assume a more gradual behavior after the initial rapid drop. The slopes of the C_{1s} and Si_{2s} signals in this region are considerably lower than the slope of the corresponding theoretical curve, which indicates an early saturation, while the slope of the O_{1s} signal exhibits a closer match to its theoretical curve. However, none of the experimental curves resembles the corresponding calculated curves for layer-by-layer growth.

The growth of GaN on sapphire appears to follow a Stranski-Krastanov mode while the growth on SiC shows some characteristics of three dimensional growth, although one would expect from the lattice mismatch a smoother growth on SiC than on sapphire. At present it is unclear whether or not this is due to the formation of a thin interfacial layer of silicon nitride.

Figure 6 shows the extinction curves of the substrate elements during UV-enhanced growth of GaN. In this case the substrate peak intensities show the same tendency to level off as they did in the first experiment, but slightly later in the growth process. In both cases however, the experimental curves drop more rapidly and subsequently show a tendency to level off before they reach zero, which is in contrast to the corresponding theoretical curves for layer-by-layer growth. As mentioned above, these curve shapes suggest island formation, either complete three-dimensional growth or Stranski-Krastanov growth. In the case of GaN growth without UV enhancement (Fig. 5), growth appears to be three-dimensional on SiC, and to follow a Stranski-Krastanov mode on sapphire with the formation of one monolayer.

In the case of UV-enhanced growth, the extinction curves for both SiC and sapphire are all similar, and indicate Stranski-Krastanov growth after the formation of 2 or 3 monolayers. Additionally, the results shown in Figure 10 reveal less evidence of silicon nitride formation than is indicated in Figure 5.

2. Growth Morphology: AlN

Figure 7 shows the change in XPS substrate peak intensities acquired during the growth of AlN. In this case, the experimental data resemble the corresponding theoretical curves more closely. This indicates that AlN grows layer-by-layer. This is in agreement with several reports which indicate that GaN films are affected beneficially when grown on an AlN buffer layer previously deposited on sapphire. Figure 8 shows the extinction curves obtained and calculated for UV-enhanced AlN growth. Here the experimental data indicate the development of island gr wth after 1 or 2 monolayers had formed. There is also more evidence of silicon nitride formation, as the C_{1s} signal drops off much more rapidly and saturates at a lower value than does the Si. As is the case with UV-enhanced growth of GaN (Fig. 6), the overall behavior of the two substrates appears to be similar.

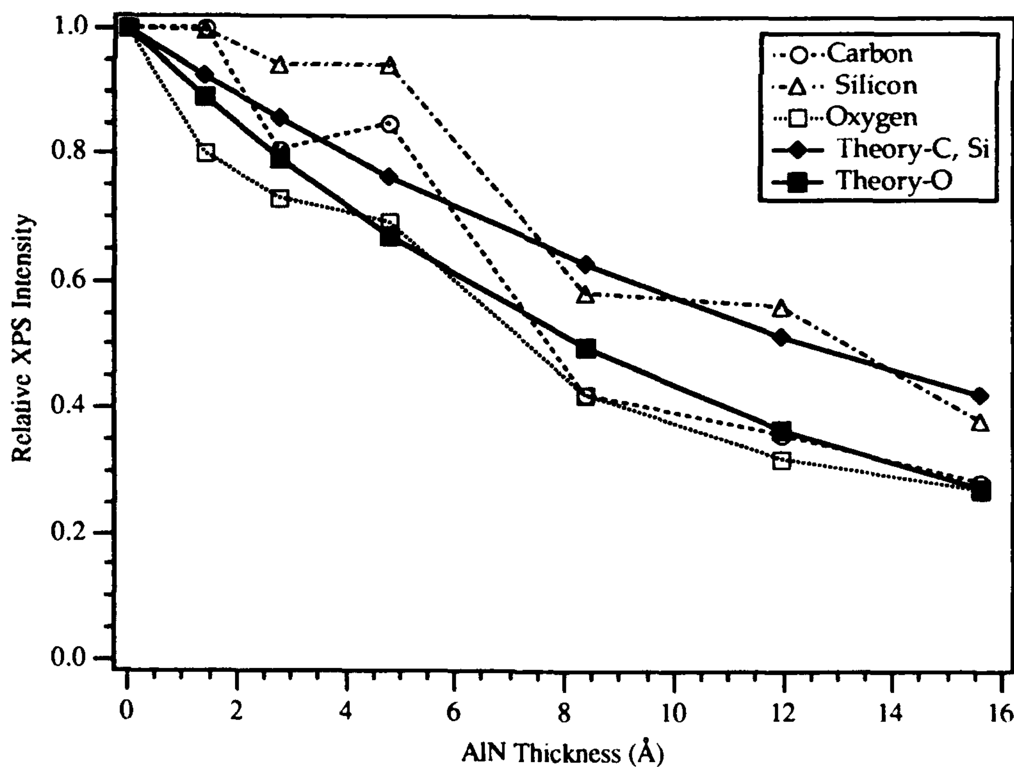

Figure 7. Change of XPS photoelectron intensity during growth of AlN on α(6H)-SiC and sapphire.

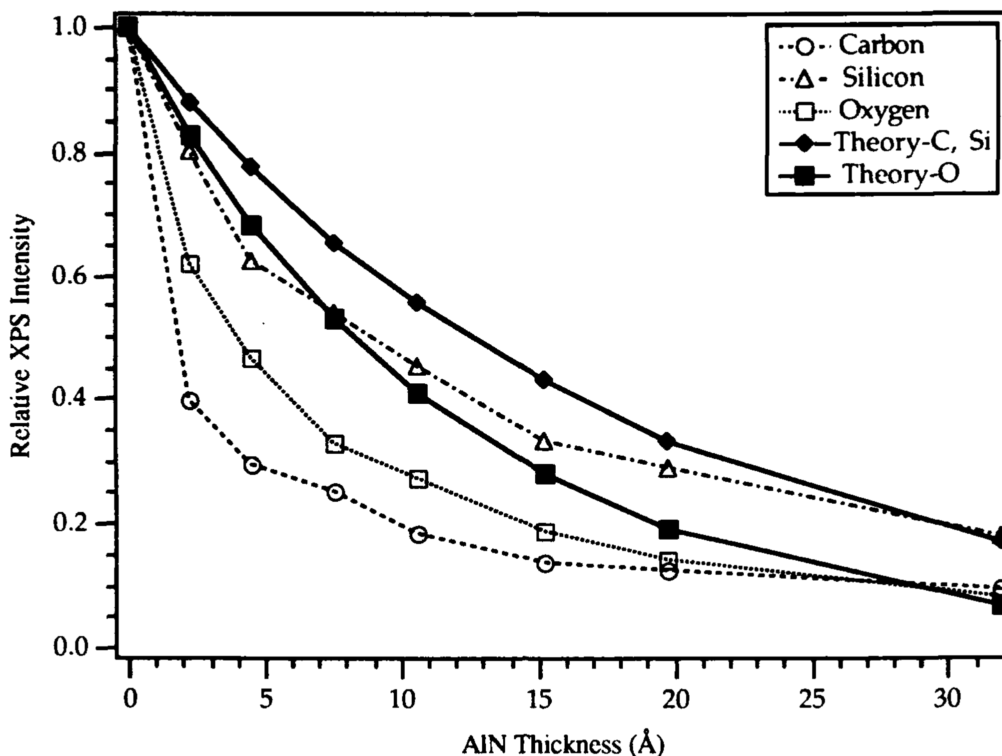

Figure 8. Change of XPS photoelectron intensity during UV-enhanced growth of AlN on α(6H)-SiC and sapphire.

3. Interface Chemistry: GaN

XPS was also used to characterize the chemical state of the substrates, interfaces and the growing films during the MBE deposition of GaN and AlN. Analysis of the cleaned substrates prior to deposition revealed the presence of very small amounts of carbon and oxygen surface contamination. The binding energy values obtained with reference to a particular peak for the growth series of GaN and AlN on sapphire and on α(6H)-SiC are listed in Tables IV, V, VI and VII.

In the case of non-UV-enhanced GaN growth (Table IV), the only XPS photopeak to show any significant binding energy shift is the Al_{2p} emission from the sapphire substrate. The slight shift (0.6 eV) may indicate that some Al-N bonding is taking place during GaN deposition, and the proportion of Al-N bonds increases with increasing coverage until the substrate is completely covered.

The Al_{2p} signal shows somewhat different behavior during the UV-enhanced growth (Table V). With the first deposition, the binding energy of the Al emission drops more than 1 eV and then gradually reaches a value similar to that in the first experiment. At the present time the reasons for this behavior are not well understood. The Ga_{3d} signal also shows a slight shift in the higher binding energy direction. The relatively low initial binding energy value for Ga is closer to the published values for elemental Ga than to GaN. This value

subsequently shifts to a higher value during deposition. It is possible that less of the Ga had reacted to form GaN in the early stages of the experiment, even though XPS peak-area calculations for Ga/N stoichiometry revealed a higher Ga/N ratio (of *total* Ga and N emission) from the first growth steps than from subsequent depositions.

Table IV. Binding energies of XPS photoelectrons measured during the GaN growth on sapphire and α(6H)-SiC.

Growth Step	0	1	2	3	4	5	6
On sapphire:							
Al_{2p}	74.0	73.8	73.6	73.4	73.7	73.4	73.4
O_{1s}	531.0*	531.3	531.1	531.0	531.2	531.0	530.9
Ga_{3d}	-	19.3	19.2	19.0	19.2	19.1	19.2
N_{1s}*	-	397.0	397.0	397.0	397.0	397.0	397.0
On α(6H)-SiC:							
Si_{2s}	152.1	152.2	152.2	152.2	152.2	152.2	152.2
C_{1s}*	283.0	283.0	283.0	283.0	283.0	283.0	283.0
Ga_{3d}	-	19.9	19.9	20.0	19.9	20.0	20.0
N_{1s}	-	397.7	397.6	397.7	397.5	397.6	397.7

* Values set as reference.

Table V. Binding energies of XPS photoelectrons measured during the UV-enhanced GaN growth on sapphire and α(6H)-SiC.

Growth Step	0	1	2	3	4	5	6
On sapphire:							
Al_{2p}	74.0	72.7	72.8	73.2	73.3	73.2	73.6
O_{1s}	531.0*	530.8	531.0	531.1	531.0	531.0	531.0
Ga_{3d}	-	18.5	18.4	18.9	18.8	18.9	19.0
N_{1s}*	-	397.2	397.2	397.2	397.2	397.2	397.2
On α(6H)-SiC:							
Si_{2p}	100.9	101.0	101.0	101.1	101.1	101.0	101.1
C_{1s}	283.0	283.0	283.0	283.0	283.0	283.0	283.0
Ga_{3d}	-	20.1	20.1	20.1	20.1	19.9	19.8
N_{1s}	-	398.0	397.9	397.9	397.8	397.7	397.5

* Values set as references; NSP = no significant peak.

Table VI. Binding energies of XPS photoelectrons measured during the AlN growth on sapphire and α(6H)-SiC.

Growth Step	0	1	2	3	4	5	6
On sapphire:							
Al_{2p}	75.0	75.0	75.0	74.8	74.5	74.2	74.1
O_{1s}	532.0*	532.2	532.1	532.0	531.9	531.8	531.8
N_{1s}*	-	397.3	397.3	397.3	397.3	397.3	397.3
On α(6H)-SiC:							
Si_{2p}	100.9	101.0	101.0	101.1	101.1	101.0	101.1
C_{1s}	283.0	283.0	283.0	283.0	283.0	283.0	283.0
Al_{2p}	-	NSP	NSP	NSP	74.0	74.0	74.1
N_{1s}	-	397.6	397.6	397.5	397.3	397.3	397.4

* Values set as references, NSP = no significant peak.

Table VII. Binding energies of XPS photoelectrons measured during UV-enhanced AlN growth on sapphire and α(6H)-SiC.

Growth Step	0	1	2	3	4	5	6	7
On sapphire:								
Al_{2p}	74.9	74.9	74.6	74.6	74.4	74.3	74.1	74.0
O_{1s}	531.9*	532.2	532.0	531.9	531.8	532.0	531.7	531.7
N_{1s}*	-	397.3	397.3	397.3	397.3	397.3	397.3	397.3
On α(6H)-SiC:								
Si_{2p}	100.7	100.8	100.9	101.0	101.0	100.9	101.2	101.0
C_{1s}	283.0	283.0	283.0	283.0	283.0	283.0	283.0	283.0
Al_{2p}	-	73.4	73.8	73.8	73.8	73.8	73.8	74.0
N_{1s}	-	397.1	397.2	397.2	397.2	397.1	397.2	397.4

* Values set as references.

4. Interface Chemistry: AlN

The binding energy values of the Al_{2p} emission during AlN growth on sapphire (Tables VI and VII) show trends similar to those seen in GaN growth. In this respect there is no difference caused by the application of UV excitation during growth. Additionally, in the case of UV-enhanced growth of AlN on SiC the Al_{2p} signal behaves in a manner similar to that of Ga_{3d} during UV-enhanced growth. The slight shift of the Al_{2p} peak from a lower binding energy value to a higher one corresponding to AlN is an indication that Al-N bonding is not complete in the earliest stages of deposition.

The sequence of Si_{2p} peaks acquired between deposition steps during the growth of AlN on α(6H)-SiC is shown in Figure 9. The initial Si_{2p} signal from the bare substrate was a symmetrical peak characteristic of clean SiC. With the first AlN growth step, significant shouldering of the peak appeared on the high binding energy side, indicating the presence of a more highly oxidized state of the silicon. This shoulder persisted throughout the film deposition process and remained as the SiC component and the overall Si intensity diminished with film growth. Gaussian curve fitting analysis was applied to the most intense shouldered peak, obtained at the first growth step, to resolve the position of the high binding energy component. The results of curve fitting are shown in Figure 10.

By means of Gaussian curve fitting, the high binding energy shouldering was found to be primarily due to a single component shifted 1.4 eV from the main SiC peak. This component has been attributed to the formation of silicon nitride during the initial stages of AlN growth. This behavior shows that the Si-face of SiC initially undergoes nitridation.

The UV-enhanced growth of AlN on SiC exhibited very similar behavior. Shouldering of the Si_{2p} peak was again quite apparent, and curve fitting of the shouldered peaks revealed the same silicon nitride component shifted 1.4 eV from the SiC peak. The results of this curve fitting for UV-enhanced growth are shown in Figure 11.

A similar conclusion could not be made for the growth of GaN on SiC, although there is little reason to expect that in this case a completely different chemistry initially occurred at the interface. The sequence of Si_{2s} peaks acquired between deposition steps during growth of GaN on α(6H)-SiC is shown in Figure 12. However, the shouldering effect was not apparent, since Si spectra obtained during the growth of GaN show lower peak intensities and a poorer signal-to-noise ratio than the spectra obtained for AlN. The close proximity of the Ga_{3s} peak on the high energy side, as shown in Figure 3, could have obscured the evidence of the silicon nitride formation as well.

The film elements Ga, Al, and N exhibited no significant changes in chemistry, except for the slight shift of the Al_{2p} peak from AlN growth on sapphire as the Al_2O_3 gave way to AlN. Thus the XPS analysis indicates that no significant chemical reactions occurred between the growing films and the substrates other than the formation of small amounts of interfacial Si_3N_4 during the initial stages of growth on SiC.

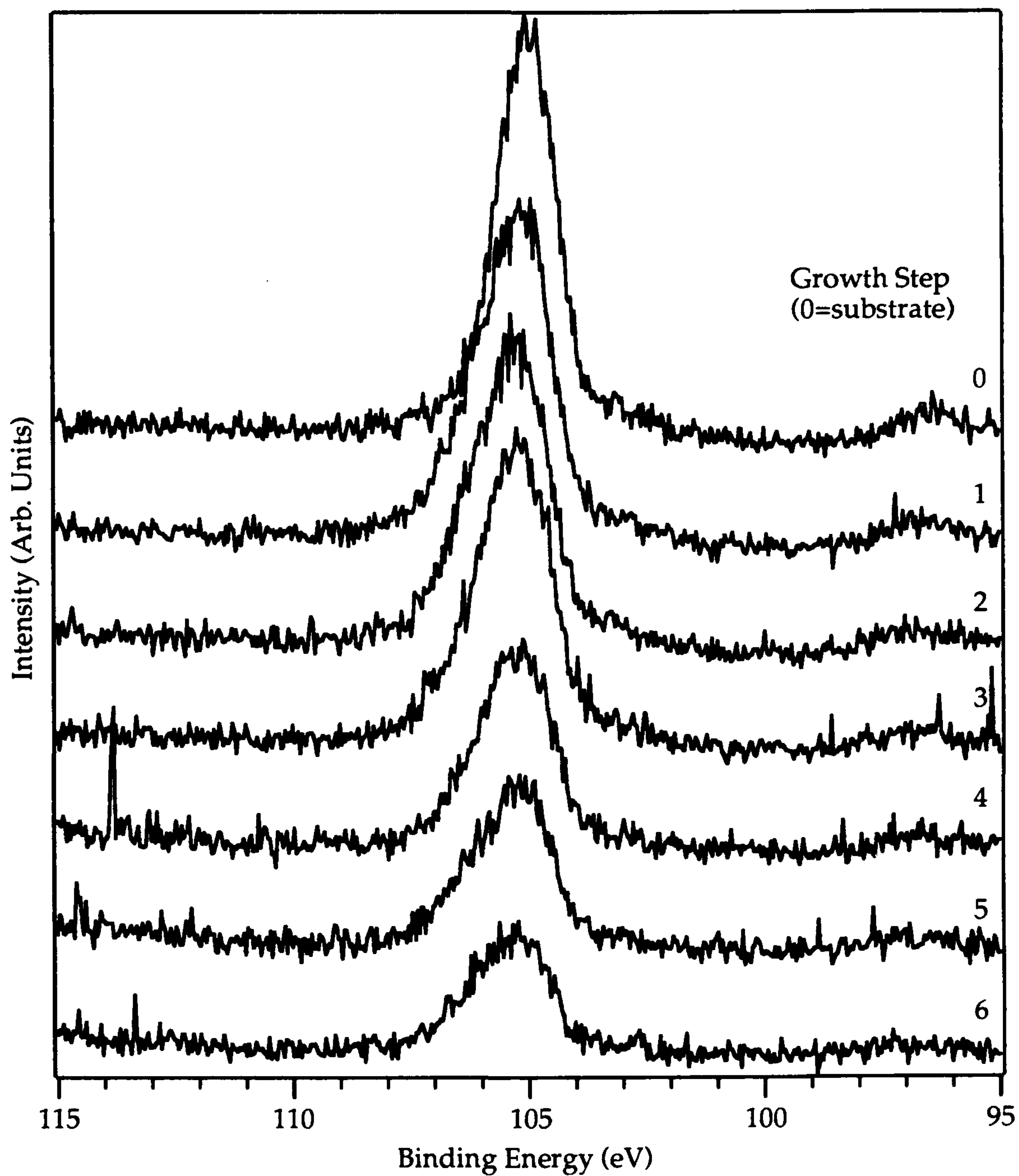

Figure 9. Si_{2p} photoemission as a function of AlN growth on SiC. Shoulder developed on the high binding energy side was due to the formation of Si_3N_4.

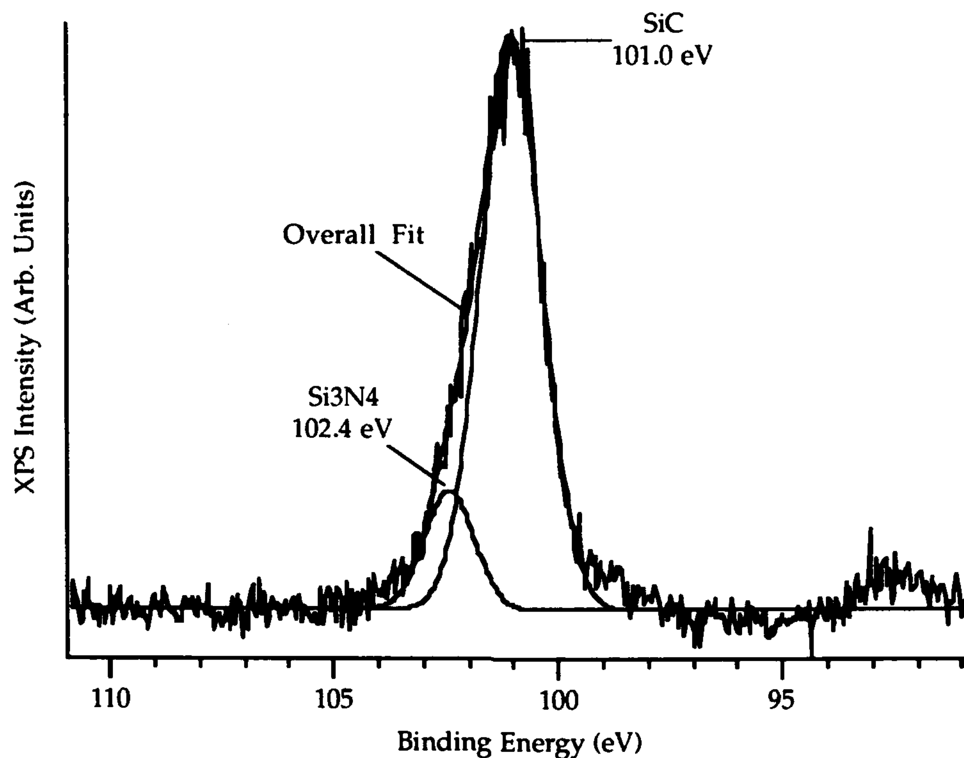

Figure 10. Gaussian curvefit of Si_{2p} photoemission from AlN deposited on α−SiC, showing component attributed to Si_3N_4 shifted 1.4 eV from SiC peak.

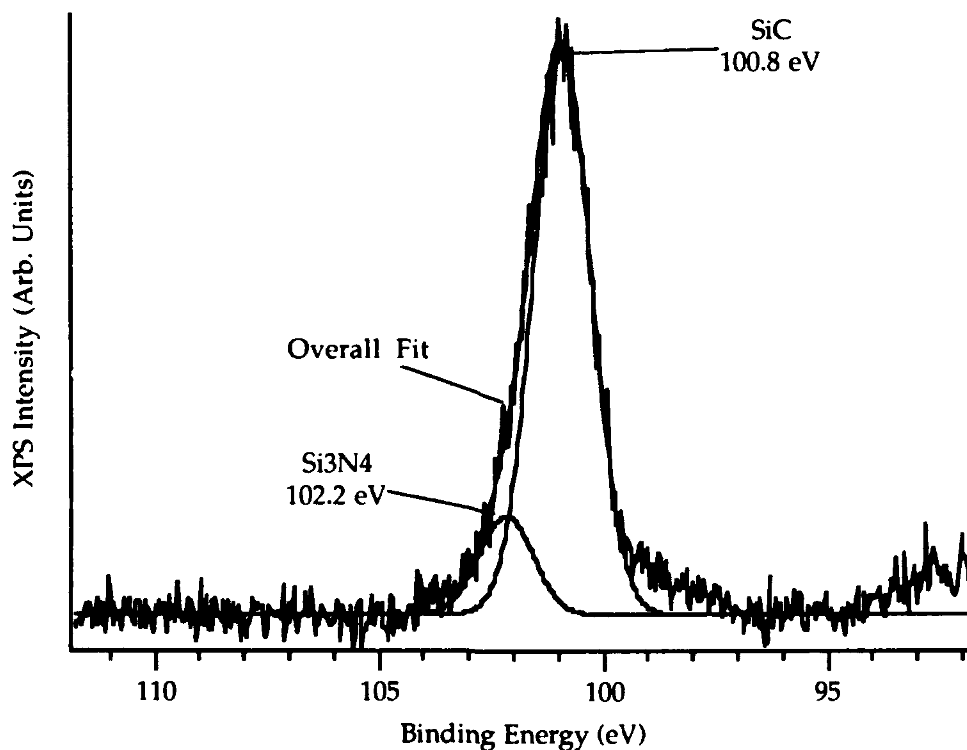

Figure 11. Gaussian curvefit of Si_{2p} photoemission from UV-enhanced deposition of AlN on α-SiC, showing Si_3N_4 component.

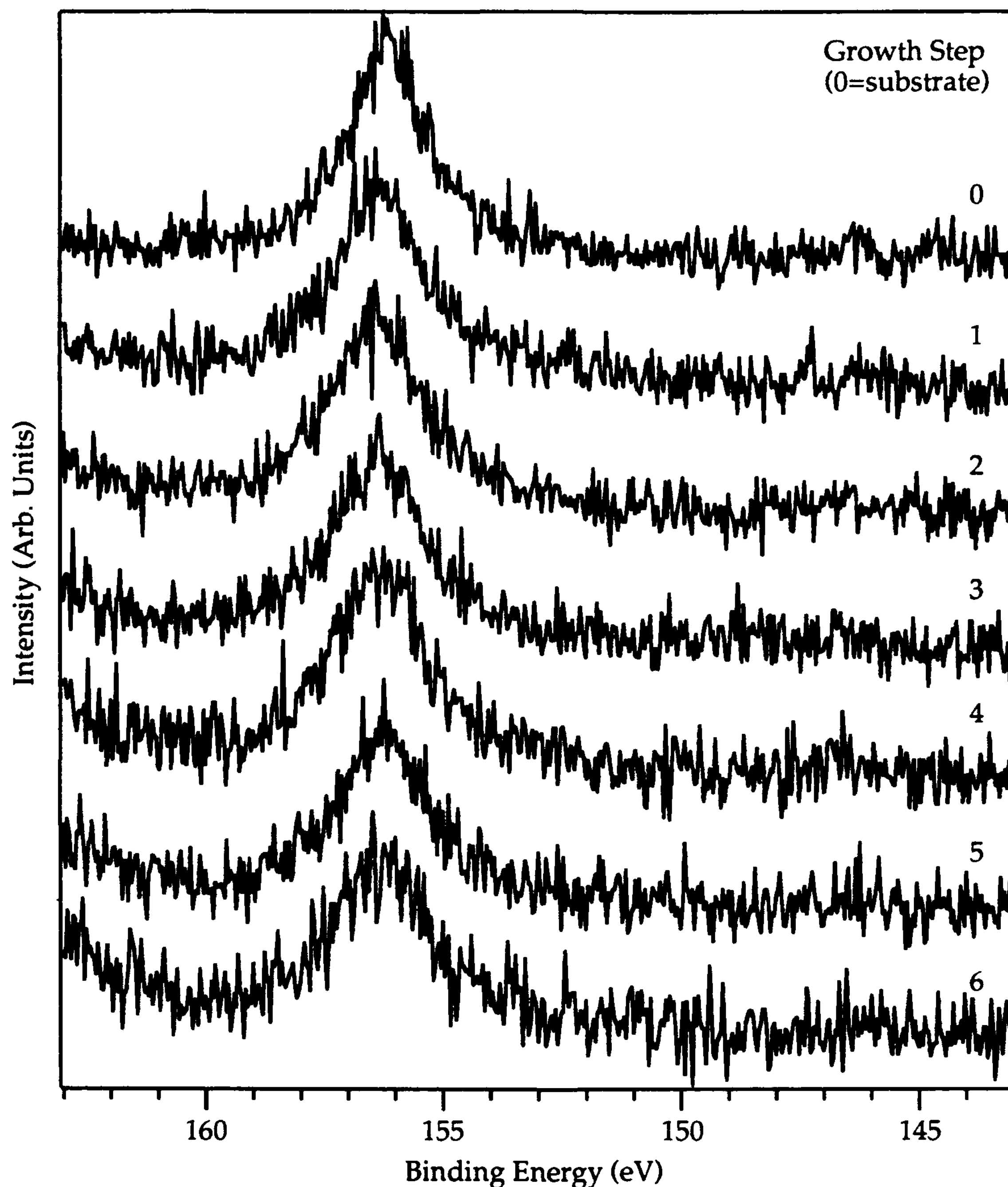

Figure 12. Si_{2s} photoemission as a function of GaN growth on SiC.

D. Conclusions

The initial stages of growth of AlN and GaN on SiC and sapphire substrates via plasma enhanced MBE and a photo-assisted MBE process were studied. Information regarding the morphology and interface chemistry was obtained. Evidence for silicon nitride formation was obtained from studies both of the Si oxidation states and the substrate peak intensity dependence on the film thickness. No significant chemical changes at the interface were observed when films were grown on sapphire.

A faster GaN nucleation was observed on SiC, while AlN apparently nucleated on both substrates equally well.

The growth of GaN on sapphire appeared to occur via the Stranski-Krastanov mode, while the growth on SiC showed some characteristics of three dimensional growth. At present, it is unclear whether or not this latter result is solely due to formation of thin interfacial layer of Si_3N_4.

The study of AlN showed that it grows layer-by-layer on both substrates. The application of UV radiation during the growth did not produce any significant changes.

E. Future Research Plans

The deposition of AlN and GaN and layered structures of these materials via GSMBE will be continued. Since the main goals are the improvement of the quality of materials, and growth of p-type GaN and AlN the short term research will be devoted to the production of smooth layers of both materials and their solid solutions. Mg will be used as the dopant for both compounds. A Hg UV light source will be to be used in the doping studies. Having achieved the quality and desired electrical properties, all efforts will be focused toward the growth of structures for simple optoelectronic devices.

F. References

1. M. R. H. Khan, Y. Koide, H. Itoh, N. Sawaki and I. Akasaki, Solid State. Comm. **60**, 509 (1986).
2. S. Yoshida, S. Misawa and S. Gonda, J. Appl. Phys. **53**, 5844 (1982).
3. Y. Koide, H. Itoh, M. R. H. Khan, K. Hiramatu, N. Sawaki and I Akasaki, J. Appl. Phys. **61**, 4540 (1987).
4. Z. Sitar, M. J. Paisley, B. Yan, J. Ruan, J. W. Choyke, and R. F. Davis, J. Vac. Sci. Technol. B **8**, 316 (1990).
5. Z. Sitar, M. J. Paisley, B. Yan, J. Ruan, J. W. Choyke, and R. F. Davis, Thin Solid Films, **200**, 311 (1991).
6 A.W. Adamson, *Physical Chemistry of Surfaces*, 5th ed. John Wiley and Sons, Inc., N.Y., 1990.
7. L.C. Feldman and J.W. Mayer, *Fundamentals of Surface and Thin Film Analysis*, North-Holland, N.Y.
8. Z. Sitar, M. J. Paisley, D. K. Smith, and R. F. Davis, Rev. Sci. Instr. **61**, 2407 (1990).
9. F. Bozso, L. Muehlhoff, M. Trenary, W.J. Choyke, and J.T. Yates, Jr., J. Vac. Sci. Technol. A **2**, 1271 (1984).
10. P.A. Taylor, M. Bozack, W.J. Choyke, and J.T. Yates, Jr., J. Appl. Phys. **65**, 1099 (1989).
11. NIST X-Ray Photoelectron Spectroscopy Database, version 1.0, NIST Standard Reference Database 20. National Institute of Standards and Technology, Gaithersburg, MD, 1989.
12. J. Hedman and N. Mårtensson, *Physica Scripta* **22**, 176 (1980).